

# Characterising the dynamics of surface water-groundwater interactions in intermittent and ephemeral streams using streambed thermal signatures

Gabriel C. Rau<sup>a,b,\*</sup>, Landon J. S. Halloran<sup>a,b</sup>, Mark O. Cuthbert<sup>a,c</sup>, Martin S. Andersen<sup>a,b</sup>, R. Ian Acworth<sup>a,b</sup>, John H. Tellam<sup>d</sup>

<sup>a</sup>*Connected Waters Initiative Research Centre, School of Civil and Environmental Engineering, UNSW Sydney, Australia*

<sup>b</sup>*Water Research Laboratory, School of Civil and Environmental Engineering, UNSW Sydney, Australia*

<sup>c</sup>*Department of Geography, University College London, United Kingdom*

<sup>d</sup>*School of Geography, Earth and Environmental Sciences, University of Birmingham, United Kingdom*

---

## Abstract

Ephemeral and intermittent flow in dryland stream channels infiltrates into sediments, replenishes groundwater resources and underpins riparian ecosystems. However, the spatiotemporal complexity of the transitory flow processes that occur beneath such stream channels are poorly observed and understood. We develop a new approach to characterise the dynamics of surface water-groundwater interactions in dryland streams using a pair of temperature records measured at different depths within the streambed. The approach exploits the fact that the downward propagation of the diel temperature fluctuation from the surface depends on the sediment thermal diffusivity. This is controlled by time-varying fractions of air and water contained in streambed sediments causing a contrast in thermal properties. We demonstrate the usefulness of this method with multi-level temperature and pressure records of a flow event acquired using 12 streambed arrays deployed along a ~12 km dryland channel section. Thermal signatures clearly indicate the presence of water and characterise the vertical flow component as

---

\*. Corresponding author : Connected Waters Initiative Research Centre & Water Research Laboratory, 110 King Street, Manly Vale NSW 2093, Australia

*Email address:* gabriel.rau@unsw.edu.au (Gabriel C. Rau)

well as the occurrence of horizontal hyporheic flow. We jointly interpret thermal signatures as well as surface and groundwater levels to distinguish four different hydrological regimes : [A] dry channel, [B] surface run-off, [C] pool-riffle sequence, [D] isolated pools. The occurrence and duration of the regimes depends on the rate at which the infiltrated water redistributes in the subsurface which, in turn, is controlled by the hydraulic properties of the variably saturated sediment. Our results have significant implications for understanding how transitory flows recharge alluvial sediments, influence water quality and underpin dryland ecosystems.

*Keywords:* surface water-groundwater interactions ; ephemeral and intermittent streams ; heat as a tracer ; hydrological characterisation ; streambed thermal regimes

---

### 1 **Highlights**

- 2 — Amplitude ratios of the daily temperature component at two different
- 3 depths in the streambed can be used to distinguish dry from saturated
- 4 sediment
- 5 — Multi-level streambed temperature records reveal distinct thermal si-
- 6 gnatures that characterize water flow
- 7 — Ephemeral or intermittent surface water-groundwater interactions can
- 8 be categorized into a sequence of hydrological regimes

## 9 1. Introduction

10 The spatial and temporal movement of water through dry stream chan-  
11 nels and the surrounding shallow sediments is highly dynamic. Stream flow  
12 cessation and drying occur in more than half of the world's river networks [1]  
13 with proportions exceeding 80% in dryland regions [2]. Water in otherwise dry  
14 channels recharges groundwater through infiltration [e.g., 3, 4, 5, 6, 7] and  
15 underpins dryland ecological diversity [e.g., 8, 2]. In fact, shallow groundwa-  
16 ter is often the only source of freshwater for human and ecosystem activity  
17 during periods of dry climate and therefore of critical importance [9, 10, 11].

18 As groundwater resources are being depleted globally [12], the largest wa-  
19 ter stresses exist in areas with high population and low surface water availa-  
20 bility [13] and are intensified by human activity [14]. Because groundwater re-  
21 charge in dryland regions is predominantly due to infiltration of water during  
22 flow events (i.e., 'focused' or 'indirect') [e.g., 9, 5], understanding temporary  
23 surface-groundwater interactions is of paramount importance [6, 7]. However,  
24 monitoring temporary flow events is challenging and thus observations are  
25 scarce [15, 16].

26 The presence of water in otherwise dry channels is generally referred to  
27 as 'ephemeral' or 'intermittent' behaviour depending on the duration of flow  
28 [e.g., 17]. When such streams are flowing, the degree of interaction bet-  
29 ween the surface and groundwater systems depends on complex hydrogeolo-  
30 gic controls [18, 19, 20]. The spatiotemporal dynamics of such surface water-  
31 groundwater interactions in these contexts are currently poorly understood  
32 [7].

33 It is recognised that streambed temperature data provides useful insight  
34 into the flow dynamics of dryland systems especially when complementing  
35 pressure data. Daily stream temperature oscillations can cause variations in  
36 stream discharge which relate to infiltration caused by the change in water  
37 physical properties [3, 21]. Constantz and Thomas [15, 22] found that stream-  
38 bed temperature can be used as an indicator of streamflow and can provide  
39 subsurface water percolation characteristics. Constantz et al. [16] and Blasch  
40 et al. [23] determined streamflow frequency and duration using streambed  
41 temperature records. Constantz et al. [24] numerically modelled subsurface  
42 temperature records and concluded that percolation rates could be constrain-  
43 ed. While much of this work, summarised in Blasch et al. [25], illustrates  
44 the temporal dynamics of transient surface-groundwater interactions, inter-  
45 pretation is limited by data from discrete spatial locations.

46 Here, we draw from the large body of heat tracing knowledge developed  
47 for surface-groundwater interactions in perennial (saturated) systems [e.g.,  
48 refer to the reviews of 26, 27, 28] and extend the methodologies to include  
49 consideration of dry systems. We exploit the fact that the presence of water in  
50 otherwise dry sediments changes the thermal properties [e.g., 15, 29, 30, 31].

51 In reality, sediments can be variably saturated, i.e. during the wetting  
52 and drying stages of a flow event. In fact, streambed sediments may never  
53 be entirely dry or fully saturated. However, we limit our analysis to realistic  
54 end-members of dry and water saturated conditions as the resulting thermal  
55 contrast is large enough to allow reliable detection of water. This simplifica-  
56 tion also avoids overly complicated saturation measurements and equations  
57 that are necessary when coupling the non-linear processes involved in vari-  
58 ably saturated conditions. For details about heat tracing to infer variably  
59 saturated processes or properties we refer the interested reader to Halloran  
60 et al. [30, 31].

61 In this paper we demonstrate that (1) streambed temperature data can  
62 be interpreted to distinguish reliably between approximately dry and satura-  
63 ted conditions below dryland streams, thus allowing identifications of stream  
64 flow episodes; (2) temperature records, interpreted using this approach, can  
65 be used to distinguish between dominantly upward, downward, and horizon-  
66 tal flow below dryland streams; (3) the qualitative results can be used to  
67 constrain conceptual models of temporary surface-groundwater interactions.  
68 Our results have significant implications for improving the evaluation of fo-  
69 cused or indirect groundwater recharge and can underpin further research on  
70 water quality and ecohydrology in dryland streams.

## 71 **2. Theoretical background**

### 72 *2.1. Propagation of diel temperature fluctuations into shallow sediments*

73 The analysis of heat tracing data utilizes the diel temperature fluctua-  
74 tions that ubiquitously occur at the Earth’s surface and propagate vertically  
75 downwards into the subsurface where the thermal wave is both damped and  
76 delayed over depth [32, 33]. For a 1D vertical section of water saturated  
77 (wet) near-surface sediment exposed to sinusoidal temperature forcing at the

78 surface, the temperature over depth and time can be described as [33, 34]

$$T^{sat}(z) = T_0 + A \cdot \exp \left[ \frac{z}{2D} \left( v - \sqrt{\frac{\alpha + v^2}{2}} \right) \right] \cdot \cos \left[ \frac{2\pi t}{P} - \frac{z}{2D} \sqrt{\frac{\alpha - v^2}{2}} \right], \quad (1)$$

79 where  $T_0$  is the ambient temperature [ $^{\circ}C$ ],  $A$  is the diel temperature ampli-  
 80 tude [ $^{\circ}C$ ],  $z$  is vertical depth [m] (positive = down),  $t$  is time [s],  $P$  is the  
 81 period of the sine wave [s],  $v$  is the thermal front velocity linearly related to  
 82 Darcy flux  $q$ . The parameter  $\alpha$  is defined as  
 83

$$\alpha = \sqrt{v^4 + \left( \frac{8\pi D}{P} \right)^2} \quad (2)$$

85 and the sediment bulk thermal diffusivity is [35, 26]

$$D = \frac{\kappa}{\rho c} \quad (3)$$

87 where  $\kappa$  is the thermal conductivity [ $Wm^{-1}K^{-1}$ ],  $\rho$  is the density [ $kgm^{-3}$ ]  
 88 and  $c$  is the specific heat capacity [ $Jkg^{-1}K^{-1}$ ] of the sediments;  $\rho c$  is the  
 89 thermal capacity [ $Jm^{-3}K^{-1}$ ] [36]. The thermal parameters depend on the  
 90 sediment moisture conditions (dry or saturated) and are discussed in Section  
 91 2.2. In this investigation we neglect thermal dispersivity as is justified for  
 92 water fluxes  $v < 10$  m/d [37].

93 Heat tracing is best conducted using a pair of temperature sensors that  
 94 are arranged vertically. The advantage is that the sensor spacing, rather  
 95 than absolute depth, can be targeted or precisely measured. In this case an  
 96 amplitude ratio can be defined for water saturated streambeds [38]

$$A_r^{sat}(\Delta z, D^{sat}, v) = \frac{A_2(z_2)}{A_1(z_1)} = \exp \left[ \frac{\Delta z}{2D^{sat}} \left( v - \sqrt{\frac{\alpha + v^2}{2}} \right) \right] \quad (4)$$

98 where  $A_1$  and  $A_2$  are the amplitude of diel temperature fluctuations measured  
 99 at discrete depths in the sediment ( $|z_2| > |z_1|$ ).

100 Analytical heat tracing has been widely used to calculate vertical water  
 101 fluxes under water saturated conditions [e.g. 27, 28]. We note that in the  
 102 case of uniform directional flow and in the absence of hydrodynamic thermal  
 103 dispersion, this approach delivers the vertical flow component of the total  
 104 flow vector [39].

105 *2.2. Heat tracing to distinguish between dry and water saturated sediments*

106 Streambed sediments can undergo variably water saturated conditions  
 107 depending on whether the channel is dry or wet, i.e. the presence of air in  
 108 the sediments [40]. Consequently, the corresponding difference in thermal  
 109 parameters must be considered. The bulk thermal diffusivity in Equation 3  
 110 has a non-linear dependency on saturation [41, 42, 31]. Côté and Konrad  
 111 [41] presented a generalized thermal conductivity model for variably satura-  
 112 ted sediment which we simplify to its dry and saturated end-members. The  
 113 thermal conductivity for dry streambeds is [41]

$$114 \quad \kappa^{dry} = \chi \cdot 10^{-\eta n} \quad (5)$$

115 where  $\chi$  and  $\eta$  are empirical parameters that depend on the grain size; here,  
 116 we use  $\chi = 1.7$  and  $\eta = 1.8$  for rocks and gravels as is most suitable for dryland  
 117 channels exposed to high energy flows;  $n$  represents the total porosity [-] of  
 118 the sediment. In contrast, the saturated thermal conductivity is given as  
 119 [43, 41, 42]

$$120 \quad \kappa^{sat} = \kappa_w^n \cdot \kappa_s^{(1-n)} \quad (6)$$

121 where subscripts  $w$  and  $s$  represent water and solid matrix, respectively.

122 The thermal capacity of a sediment with two phases (dry : air and solid  
 123 matrix, saturated : water and solid matrix) is defined as a porosity weighted  
 124 volumetric mean [44, 36, 31]

$$125 \quad (c\rho)^{dry} = (1 - n)(c\rho)_s \quad (7)$$

$$126 \quad (c\rho)^{sat} = n(c\rho)_w + (1 - n)(c\rho)_s \quad (8)$$

127 where subscripts  $w$  and  $s$  represent water and solid matrix, respectively. The  
 128 specific heat capacity of air is so small that it can be neglected in our analysis  
 129 [31].

130 Thermal diffusivity for water saturated ( $D^{sat}$ ) and dry ( $D^{dry}$ ) sediment  
 131 can be calculated by using Equation 3 in combination with Equations 6 and  
 132 8 or Equations 5 and 7, respectively.

133 Under the conditions of water saturated streambed sediments, the am-  
 134 plitude ratio  $A_r^{sat}$  (Equation 4) is a function of the bulk saturated thermal  
 135 diffusivity of the sediment  $D^{sat}$  and the thermal front velocity (determined  
 136 by the vertical flow of water),  $A_r^{sat}(D^{sat}, v)$ . For dry streambed sediments,  
 137 the amplitude ratio will only depend upon the bulk dry sediment thermal  
 138

139 diffusivity  $D^{dry}$  because the absence of water also means that  $v = 0$  (no flow).  
 140 Consequently, under dry conditions Equation 4 can be simplified to

$$141 \quad A_r^{dry}(\Delta z, D^{dry}) = \frac{A_2(z_2)}{A_1(z_1)} = \exp \left[ -\Delta z \sqrt{\frac{\pi}{PD^{dry}}} \right]. \quad (9)$$

142 This equation can be reformulated to calculate the dry bulk sediment ther-  
 143 mal diffusivity  $D^{dry}$  from the ratio of the diel temperature amplitudes mea-  
 144 sured using two sensors located at different depths during a period when the  
 145 streambed is dry.

146 In reality, streambed thermal properties and porosity can vary within natu-  
 147 ral limits. Significant effort towards additional field measurements would  
 148 be required to constrain these parameters, as the phase shift of the thermal  
 149 wave cannot be used to separate the sediment thermal conductivity or spe-  
 150 cific heat capacity from thermal diffusivity. Note also that calculation of the  
 151 saturated streambed thermal diffusivity is hindered by the degree of freedom  
 152 introduced through a variable vertical water flux and is therefore impossible  
 153 to accomplish without independent flow measurements.

154 To determine whether there is always a difference in amplitude ratio for  
 155 dry and saturated sediments, given the range of natural parameter variabi-  
 156 lity, we evaluated  $\Delta A_r^{dry,sat} = A_r^{sat} - A_r^{dry}$  as a function of the respective  
 157 thermal diffusivity values. Note that for a given location in space, the ther-  
 158 mal properties of the solid matrix, as well as the porosity, remain constant  
 159 during any change from dry to saturated. While the thermal property values  
 160 for water are accurately defined (Table 1), the three unknown properties are :  
 161 The streambed porosity  $n$  (which we allow to vary between 0.2 and 0.5), solid  
 162 thermal conductivity  $\kappa_s$  (low porosity volcanic rocks [46]), and solid thermal  
 163 capacities  $(c\rho)_s$  (rock forming minerals [36]).

164 Figure 1a shows the resulting  $\Delta A_r^{dry,sat}$  as multi-parameter space at dis-  
 165 crete values of porosity over the range of thermal parameters. This illustrates  
 166 that the diel temperature amplitude is significantly different for a realistic  
 167 range of dry and water saturated streambed sediments,  $A_r^{dry} < A_r^{sat}$ . This is  
 168 because during a flow event the streambed pore space, initially occupied by  
 169 air, will be replaced with water with significantly different thermal proper-  
 170 ties. A change in  $A_r$  can, therefore, be used to distinguish between realistic  
 171 end-members of water saturation (dry vs. saturated), and therefore acts as  
 172 an easily measurable proxy for streambed flow processes.

Parameter/Phase	Unit	Parameter range			References	
		$P_{10}$	$-2\sigma$	$\mu$		$+2\sigma$
Porosity	Total pore space $n$		0.2	0.35	0.5	
Water	Thermal conductivity $\kappa_w$	$Wm^{-1}K^{-1}$		0.6		a
	Specific heat capacity $c_w$	$Jkg^{-1}K^{-1}$		4185		a
	Density $\rho_w$	$kgm^{-3}$		998		a
Solid matrix	Thermal conductivity $\kappa_s$	$Wm^{-1}K^{-1}$	1.62	3.08	4.54	b
	Thermal capacity $(\rho c)_s$	$MJm^{-3}K^{-1}$	1.8	2.45	3.1	c
	Density $\rho_s$	$kgm^{-3}$		2650		
Thermal diffusivity	Dry streambed	$m^2s^{-1}$	$1.79 \cdot 10^{-7}$	$2.61 \cdot 10^{-7}$	$3.57 \cdot 10^{-7}$	
	Saturated streambed	$m^2s^{-1}$	$4.04 \cdot 10^{-7}$	$5.73 \cdot 10^{-7}$	$7.67 \cdot 10^{-7}$	

TABLE 1: Thermal parameters used for the *Monte-Carlo* analysis to assess the difference between dry and saturated amplitude ration as a function of streambed thermal diffusivity. References : a) NIST [45]. b) Clauser [46]. c) Waples and Waples [36].

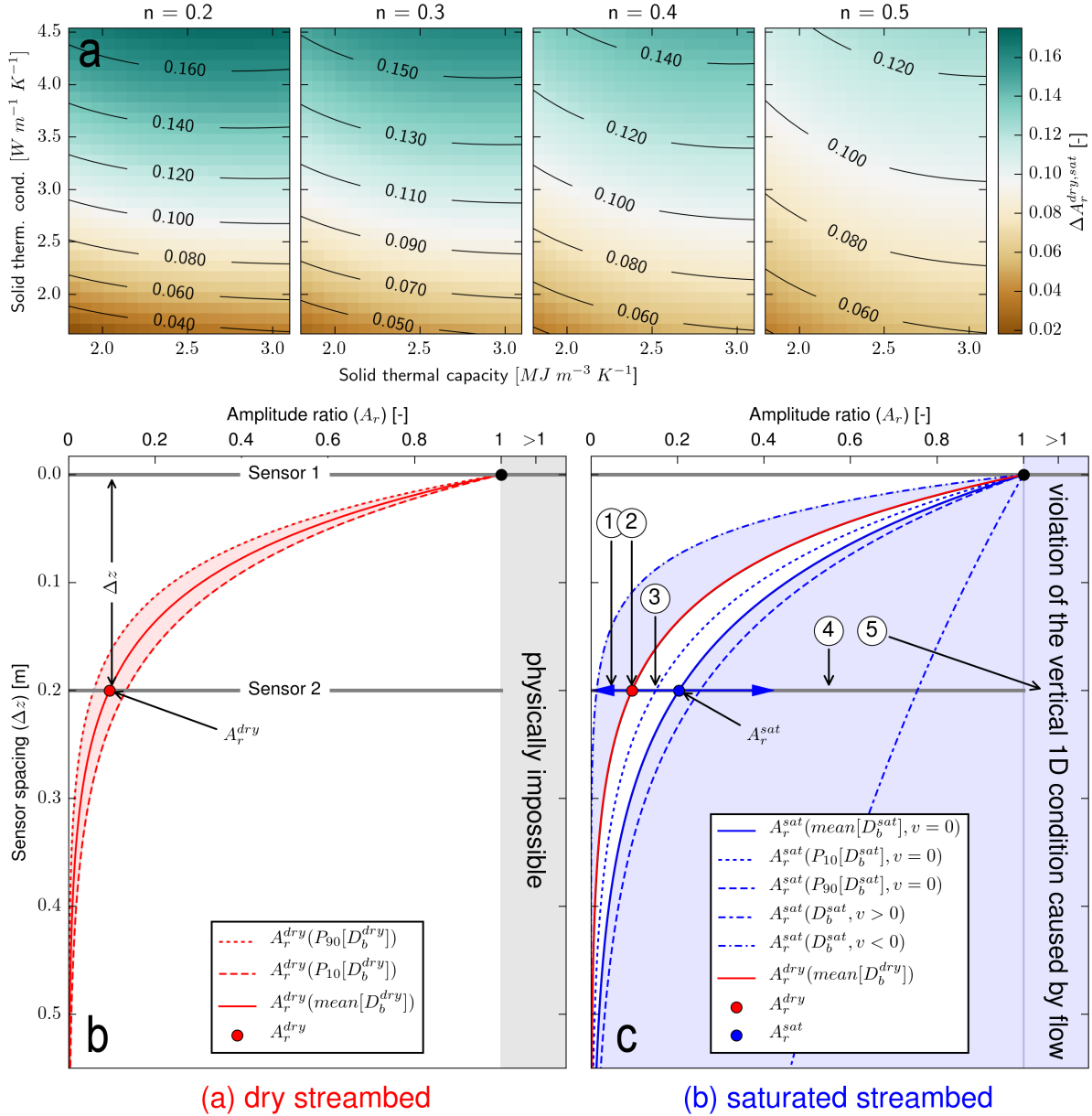


FIGURE 1: Conceptual model illustrating how to characterize the dynamics of ephemeral surface-groundwater interactions in shallow variably saturated sediments using the diel temperature amplitude ratio ( $A_r$ ) as a signature : a) The likely range of the diel temperature amplitude ratio for dry and saturated streambeds (resulting from a range of porosity and thermal parameters) is shown for an example sensor spacing  $\Delta z = 0.2$  m and thermal front velocities of  $v = \pm 1$  m/d. b) The thermal diffusivity of wet streambed sediments is different leading to a change in amplitude ratio during flow. Further, changes in amplitude ratio can indicate the vertical direction of water fluxes in the sediments between the temperature sensors. This can be used to characterise ephemeral surface-groundwater interactions during flow events. c) The difference between dry and saturated ( $v = 0$ ) amplitude ratio  $\Delta A_r$  as a function of a range in solid thermal conductivity  $\kappa_s$  and solid thermal capacity  $(\rho c)_s$  at discrete porosity values. Numbered labels 1-5 are explained in the text.

173 2.3. *Shallow streambed thermal signatures detect water and characterize flow*  
 174 *through variably saturated streambed sediments*

175 To estimate the saturated streambed thermal diffusivity  $\Delta A_r^{dry,sat}$  can be  
 176 used. We performed a *Monte-Carlo* analysis (100,000 samples) to establish  
 177 the most likely values for dry and saturated amplitude ratio as a function  
 178 of streambed thermal diffusivity. We use the literature derived ranges shown  
 179 in Table 1 as input assuming that all properties follow a normal distribution  
 180 and that 95.4% of the existing values fall within these limits (i.e.,  $\mu \pm 2\sigma$ ).  
 181 The resulting mean and percentile ( $P_{10}$  and  $P_{90}$ ) values for dry and saturated  
 182 streambed thermal diffusivity are listed in Table 1. These values were used  
 183 to plot the amplitude-depth relationships in Figure 1b and 1c and visualise  
 184 the difference between dry and saturated  $A_r$ .

185 Figure 1 demonstrates that the  $A_r$  can be divided into the following ca-  
 186 tegories (see corresponding labels in Figure 1c) :

- 187 (1)  $0 < A_r(t) < A_r^{dry}$  : Water saturated sediment and a vertical upward  
 188 flow component.
- 189 (2)  $A_r(t) = A_r^{dry}$  : Dry end-member of the streambed sediments which can  
 190 be established from temperature records acquired during dry periods.
- 191 (3)  $A_r^{dry} < A_r(t) \leq A_r^{sat}$  : A small range of ambiguity where the exact  
 192 conditions are unclear, i.e. variable water saturation or fully saturated  
 193 with a flow component ranging between vertical upward and zero. Here,  
 194 *Monte-Carlo* analysis offers a measure of the uncertainty to compare  
 195 with the difference between  $A_r^{dry}$  and  $A_r^{sat}$  ( $0.02 < \Delta A_r < 0.175$ , Figure  
 196 1a). We note that interpretations can still be made when temperature  
 197 data are acquired in conjunction with pressure, as values are indicative  
 198 of the presence of water above the point of measurement.
- 199 (4)  $A_r^{sat} < A_r(t) \leq 1$  : Water saturated sediment and larger values for an  
 200 increasing vertical downward flow component.
- 201 (5)  $A_r(t) > 1$  : Water-saturated sediment and conditions that violate the  
 202 1D vertical flow assumption inherent to Equation 1. This has been  
 203 observed previously [47] and can, in the absence of a daily fluctuating  
 204 subsurface heat source, only be caused by horizontal hyperheic flow.

205 To simplify the approach we only consider the end-members of saturation,  
 206 close to dry and water saturated. In reality, there could be variable saturation  
 207 in the streambed sediments, particularly during the onset of flow and drying

208 of the channel. During times of variable water saturation, the amplitude ratio  
 209 will be between  $A_r^{dry}$  and  $A_r^{sat}$ .

210 Figure 1 clearly illustrates that under realistic conditions, the saturated  
 211 amplitude ratio  $A_r^{sat}$  (Equation 4) should always be larger than the dry  
 212 amplitude ratio  $A_r^{dry}$  (Equation 9), i.e.  $\Delta A_r > 0$ . The diel amplitude ratio  $A_r$ ,  
 213 therefore, allows detection of the moisture state, i.e. dry or saturated, as well  
 214 as characterization of vertical water movement through sediments when the  
 215 system is near the saturated end-member.

216 In this method we abstain from quantifying infiltration rates because  
 217 this would require knowledge of the streambed moisture content during flow  
 218 events as well as the associated thermal diffusivity. In our approach, the zone  
 219 of  $A_r$  ambiguity due to variable moisture content occupies values representa-  
 220 tive of saturated conditions and upward water flow. Given that streams with  
 221 temporary flow are generally hydraulically disconnected from the ground-  
 222 water table [e.g. 48, 6], water will most likely percolate downwards at least  
 223 as long as a variably saturated zone remains. Under these conditions,  $A_r(t)$   
 224 should serve as a novel indicator revealing the streambed processes during  
 225 ephemeral or intermittent flow.

#### 226 2.4. Extraction of the diel amplitudes from temperature measurements

227 Equation 1 requires that the temperature forcing is a sinusoidal wave.  
 228 This is not a realistic assumption under real-world conditions. However, we  
 229 can capitalise on the fact that any signal can be decomposed into a finite  
 230 sum of sinusoidal components using the *Discrete Fourier Transform*. This is  
 231 necessary so that the resulting signal component complies with the condi-  
 232 tions inherent to Equation 1, and that the amplitude of a single frequency  
 233 component (e.g., daily) can be used directly with  $A_r$  in Equations 4 and 9.

234 To calculate diel temperature amplitudes a *Fast Fourier Transform* (FFT),  
 235 as implemented in *Python*, can be applied to subsets of the data which span  
 236 a multiple number of days. The FFT of a signal is defined as

$$237 \quad \hat{s}(f_k) = \mathcal{F}\{s(t_n)\} = \sum_{n=0}^{N-1} s(t_n) e^{-2\pi i k n / N} \quad (10)$$

238 where  $k$  and  $n$  denote the indices of discretely sampled frequency and time,  
 239 respectively, which range from 0 to  $N-1$ . It is not important to normalize the  
 240 transform as long as data treatment is consistent and ratios of the amplitudes

241 are used. The discrete frequencies of the transformed signal are

$$242 \quad f_k = kf_s/N. \quad (11)$$

243 For a window of  $i$ -multiple days, the absolute value of the  $i$ -th entry  $f_i$

$$244 \quad A(f_i) = |\hat{s}(f_i)| = \sqrt{\mathcal{R}^2(f_i) + \mathcal{I}^2(f_i)} \quad (12)$$

245 corresponds to the amplitude of the  $f = 1$  cpd (cycles per day) frequency  
246 component [30]. This procedure is repeated as a rolling window along the time  
247 series whereby  $A(f_i)$  is allocated to the time at the center of the window.

248 Using this approach, a temperature amplitude time series can be extrac-  
249 ted and used to calculate amplitude ratios from Equation 4. Ephemeral flow  
250 events can be characterised using the methodology described earlier. It is  
251 important to neglect extracted amplitude values that are below the tem-  
252 perature resolution of commonly available sensors, i.e.  $A > 0.01^\circ C$  can be  
253 considered valid. Theoretically, the component phases could also be extrac-  
254 ted and used. However, Rau et al. [49] noted that signal non-stationarity, as  
255 inherent in natural temperature oscillations, causes erroneous phase results  
256 which significantly decreases the accuracy of any phase-derived calculations.

### 257 **3. Field example from Middle Creek in the Maules Creek Catch-** 258 **ment, New South Wales, Australia**

#### 259 *3.1. Catchment context*

260 The Maules Creek catchment is located in the semi-arid northwestern area  
261 of New South Wales (NSW), Australia (Figure 2). Middle Creek flows into  
262 Horsearm Creek, then Maules Creek and further into the Namoi River which  
263 is a tributary of the large Murray-Darling Basin (MDB) (Figure 2). The  
264 Nandewar range provides the northern and eastern margin of the catchment  
265 and consists of Miocene basaltic mountains peaking at 1,506 m (Mt. Kaputar)  
266 Australian Height Datum (AHD). The Namoi River at the western part of  
267 the catchment is at approx. 230 m AHD. The difference in topography causes  
268 a significant orographic rainfall effect resulting in a long-term average rainfall  
269 of 928 mm/a in the mountains (Mt. Kaputar at 1450 m AHD) and 561 mm/a  
270 on the floodplain (Narrabri Bowling Club at 229 m AHD and only 35 km  
271 west of Mt. Kaputar).

272 A major change in geology separates the Carboniferous and Devonian  
273 rocks in the upper catchment from the Permian lower catchment. The Car-  
274 boniferous and Devonian metasediments and intrusives have been thrust over

275 the Permian Mauls Creek coal measures to the west with the thrust zone oc-  
276 ccurring at the mountain front between T11 and T10 (Figure 2). The high  
277 energy flows from the mountains have cut 10 to 15 m deep channels into the  
278 coal measures that are now filled with a very heterogeneous assemblage of  
279 boulders, sand and gravels that are substantially reworked by each major  
280 flood.

281 This catchment area has been well instrumented for groundwater moni-  
282 toring since 2009 through the Australian Government National Collabora-  
283 tive Infrastructure Strategy (NCRIS). A number of research projects were  
284 conducted mainly in the lower part of the catchment : Andersen and Ac-  
285 worth [50] surveyed the perennial surface-groundwater interactions and no-  
286 ted the complexity of these processes. Rau et al. [47] successfully quantified  
287 the rate of saturated vertical flow in the streambed using heat as a tracer. To  
288 evaluate the groundwater resources within the catchment, a comprehensive  
289 groundwater model was created and illustrated considerable uncertainty and  
290 a lack of information about groundwater recharge through the intermittent  
291 stream channels originating at the mountain front [51]. Further research on  
292 groundwater resources as well as surface water-groundwater interactions can  
293 be found in McCallum et al. [52], Kelly et al. [53] and Cuthbert et al. [7].

### 294 *3.2. Monitoring of rainfall, groundwater and streambed water levels and tem-* 295 *perature*

296 Middle Creek drains an estimated  $106 \text{ km}^2$  of the upper catchment and  
297 the discharge point of which is located at the confluence with Horsearm Creek  
298 (Figure 2). Rainfall was recorded at weather stations using tipping bucket  
299 rain gauges (Campbell Scientific Inc., USA) at three different locations (see  
300 abbreviations in Figure 2b) : Mt Kaputar National Park (MK, Australian  
301 Government Bureau of Meteorology station #54151), Middle Creek Farm  
302 (MCF) and Bellevue Farm (BVF). An additional long-term rainfall dataset  
303 is available from the Mount Lindsay Station (ML, Australian Government  
304 Bureau of Meteorology station #54021) which has been operational since  
305 1886 and located  $\sim 11$  km south-east of the Mt. Kaputar station. The Mount  
306 Lindsay Station has an elevation of  $\sim 870$  m but lies in a rain shadow of the  
307 higher Mt. Kaputar rain gauge.

308 The loggers used to measure streambed temperature and pressure were a  
309 combination of off-the-shelf devices : HOBO temp pro v2 (U22-02), Schlum-  
310 berger Diver and Solinst Levelogger Gold/Edge. The temperature measured  
311 by the loggers was calibrated against a reference (Fluke hand-held 1524) in

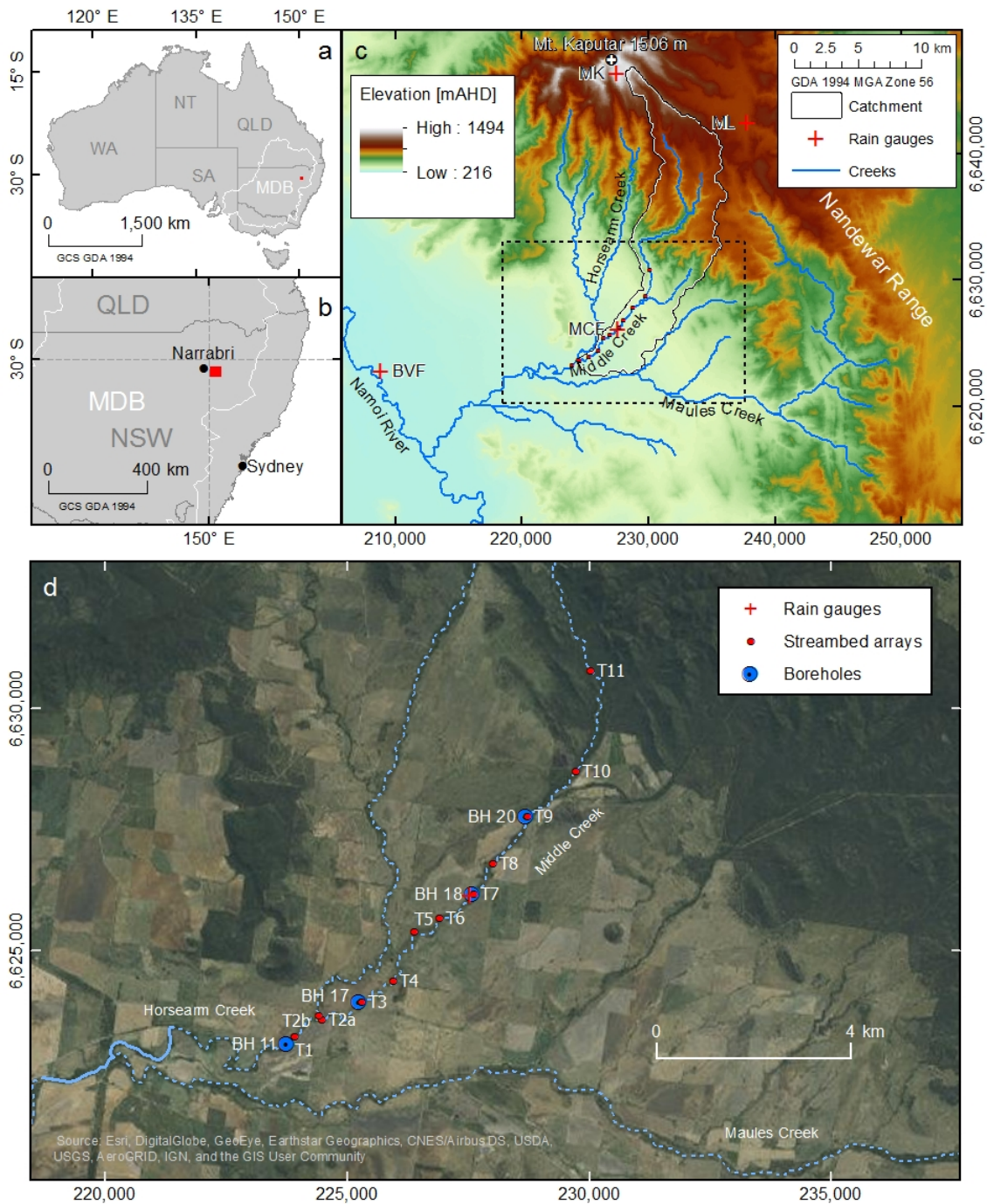


FIGURE 2: Map showing (a) the location the Maules Creek catchment in relation to the Murray-Darling Basin (MDB), (b) the state of New South Wales, (c) a catchment elevation map with locations of rain gauges, (d) streambed array installations and piezometers along Middle Creek.

312 a bucket of well-stirred water at different values. The calibration was applied  
313 as a correction to the temperature field records.

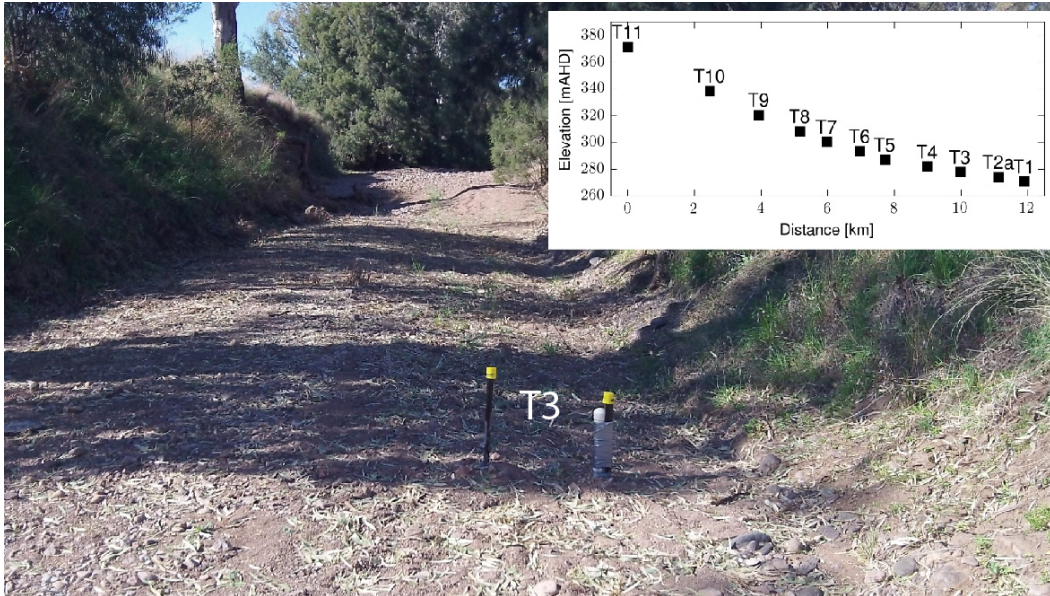


FIGURE 3: Streambed array T3 installed in the dry channel as an example representative of the other locations. Inset plot shows the distance-elevation profile for all arrays as surveyed using differential GPS (Table 2).

314 Temperature and pressure were recorded at discrete depths in the shallow  
315 streambed at a total of 12 different locations along Middle Creek. Multi-level  
316 streambed arrays were constructed from 32 mm diameter standard hydraulic  
317 PVC pipe. Loggers were placed inside the pipe at defined intervals (multi-  
318 level monitoring), with the pressure measured at the top and bottom end,  
319 and separated by spacers [47, 54]. The effect of this array design on the  
320 measured diel amplitudes has been found to be negligible [55]. The length of  
321 the streambed arrays depended on the number of loggers used at the different  
322 locations of deployment. Table 2 contains the details of the streambed arrays.

323 Because the stream flow events can be high energy, installation of the  
324 arrays required the construction of an anchor point. At each location, two  
325 star pickets were manually driven into the streambed sediments in an x-  
326 formation and a small pit was dug around the point of contact between the  
327 star pickets. The pit was then filled with quick-set concrete and covered with

328 large cobbles. For an example installation please refer to Figure 3.

329 Short arrays were directly attached to the star pickets with the uppermost  
330 sensor located at the same vertical level as the streambed. Longer, multi-  
331 level arrays were installed with the same method as described by [47] at  $\sim 1$   
332 m downstream and securely attached to the anchor point. Streambed arrays  
333 were installed at the end of July 2013, and loggers were programmed to record  
334 pressure and temperature at 15 min intervals. The aim was to capture an  
335 entire flow event along the creek.

336 Geospatial coordinates of all installation points were accurately surveyed  
337 using differential GPS equipment (Trimble R10 GNSS). For a summary of  
338 streambed monitoring arrays, measured parameters and locations refer to  
339 Table 2. An atmospheric pressure record, obtained from the MCF weather  
340 station, was used to calculate gauge pressure and hydraulic heads in combi-  
341 nation with the survey. The approximate flow distance between the first and  
342 last monitoring points was traced in *ArcMAP* based on an identification of  
343 the channel from satellite imagery and is reported in Table 2.

344 Multi-level boreholes were installed right next to the ephemeral stream  
345 channel (distance within tens of meters) as described by Cuthbert et al. [7].  
346 To determine the hydraulic connectivity between surface flow and ground-  
347 water in the sediments along the channel (BH 11, BH 17, BH 18 and BH 20  
348 in Figure 2d), the shallower screens were monitored at 15 min intervals.

### 349 *3.3. Spatiotemporal surface and groundwater responses to a major rainfall* 350 *event*

351 Cumulative rainfall of 329 mm, 198 mm and 228 mm was measured at  
352 MK, MCF and BVF, respectively, for the 60-day period from 20 March to 18  
353 May 2016 (4a). This rainfall occurred as clustered rain events with short per-  
354 iods of dry weather. The rainfall triggered mountain run-off and led to stream  
355 flow along the channel as recorded by the streambed arrays summarised in  
356 Figure 4. The rainfall amount was more than double the average long-term  
357 (1886-2012) moving 60-day sum of 155 mm (max. 809 mm in February 1971),  
358 indicating that it was a sizeable event for this catchment.

359 Figure 4 summarises the dynamics of water movement along Middle  
360 Creek, over depth and in time for this event. Note that the array (streambed  
361 surface) elevations almost perfectly follow an exponential curve (inset in Fi-  
362 gure 3 based on data in Table 2). The run-off moved along the previously dry  
363 channel and was captured by the pressure transducers at the streambed as a  
364 hydrograph peak with differing heights. Water levels upstream (array T11)

Array	Elevation [m]	Distance [m]	Intervals	Parameters	Length [m]	$\Delta z$ [m]	Mean $A_r^{dry}$ [-]	Stdev $A_r^{dry}$ [-]	$D^{dry}$ [ $m^2/s$ ]
T11	371.59	0	2	p & T	0.230	0.235	0.212	0.017	8.35E-07
T10	338.57	2,464	2	p & T	0.173	0.173	0.435	0.020	1.57E-06
T9	320.69	3,934	6	p & T	1.129	0.190	0.281	0.033	8.16E-07
T8	308.36	5,167	2	T	0.200	0.200	0.289	0.022	9.44E-07
T7	300.65	5,976	5	p & T	1.158	0.190	0.286	0.025	8.38E-07
T6	293.61	6,970	2	p & T	0.173	0.173	0.413	0.019	1.39E-06
T5	287.37	7,712	2	T	0.200	-	-	-	-
T4	281.87	8,992	2	p & T	0.173	0.173	0.290	0.013	7.12E-07
T3	278.00	9,979	5	p & T	1.060	0.190	0.222	0.027	5.79E-07
T2a	274.21	11,125	2	p & T	0.240	0.200	0.211	0.011	6.00E-07
T2b	274.94	-	2	p & T	0.200	0.240	0.211	0.018	8.65E-07
T1	271.14	11,903	2	p & T	0.171	0.173	0.206	0.015	4.35E-07

TABLE 2: streambed monitoring arrays and locations in order of distance along the flow direction. Projected coordinates are the same as in Figure 2. Abbreviations p and T stand for pressure transducer and temperature sensor, respectively.

365 peaked on 28 Mar 2014 at 4 :15. The flood took 135 min to move  $\sim 11.9$  km  
366 (Figure 2) to the downstream end (array T1) with an average velocity of  
367  $\sim 1.5$  m/s. Note that array T8 and T5 did not contain pressure transducers.

368 The depth to groundwater (thickness of the unsaturated zone) along the  
369 stream channel (between BH20 and BH11) was variable before the flow event  
370 and generally decreased in the downstream direction. The shallow ground-  
371 water responds immediately to stream flow illustrating infiltration of surface  
372 water into the alluvial sediments and demonstrating an evolving connection  
373 between surface and groundwater [19, 56, 57].

374 The groundwater hydrograph responses vary at the four locations along  
375 the channel. For example, in the downstream locations (from T3 and BH 17  
376 to T1 and BH 11) the rapid movement of infiltrating surface water to the  
377 water table causes a peak in groundwater levels within days of the flow event  
378 followed by a steady decline. This is consistent with the conceptual model  
379 of groundwater redistribution beneath transitory streams that has been de-  
380 veloped by Cuthbert et al. [7] and can be described by the aquifer response  
381 time (ART) defined as  $t_{ART} = \frac{L^2 S_y}{2T}$ , where  $L$  is a given length,  $S_y$  is specific  
382 yield and  $T$  is transmissivity. In contrast, the subsurface water mound up-  
383 stream (from T9 and BH 20 to T7 and BH 18) increases and redistributes  
384 much more slowly as a temporary hydraulic connection to the groundwater  
385 is established [19]. Our water level measurements, when interpreted using  
386 results from a systematic numerical investigations of variations in ground-  
387 water head in response to surface flow [57], reveal that hydraulic properties  
388 of the alluvium are highly heterogeneous. For example, the responses mea-  
389 sured upstream (BH18 and BH20) indicate that a low-permeability layer (or  
390 clogging layer) may exist beneath the stream and that the average hydraulic  
391 conductivity is lower compared to the downstream sites (BH11 and BH17).

392 The slower redistribution of water in the shallow aquifer results in far  
393 more prolonged surface flow than in the lower catchment. Note that the  
394 initially sharp rise in heads recorded at BH20 during the first few days of the  
395 flow event is likely due to a loading effect with the more gradual rise that  
396 follows being due to groundwater recharge due to streambed infiltration and  
397 lateral movement of groundwater.

398 Interestingly, the surface water hydrograph after the flood peak behaves  
399 differently for each array along the flow path (Figure 4). The upstream arrays  
400 show a gradual hydrograph flattening after the initial peak, followed by a  
401 stable water level for a period of time which spanned from  $\sim 3$  to 6 weeks

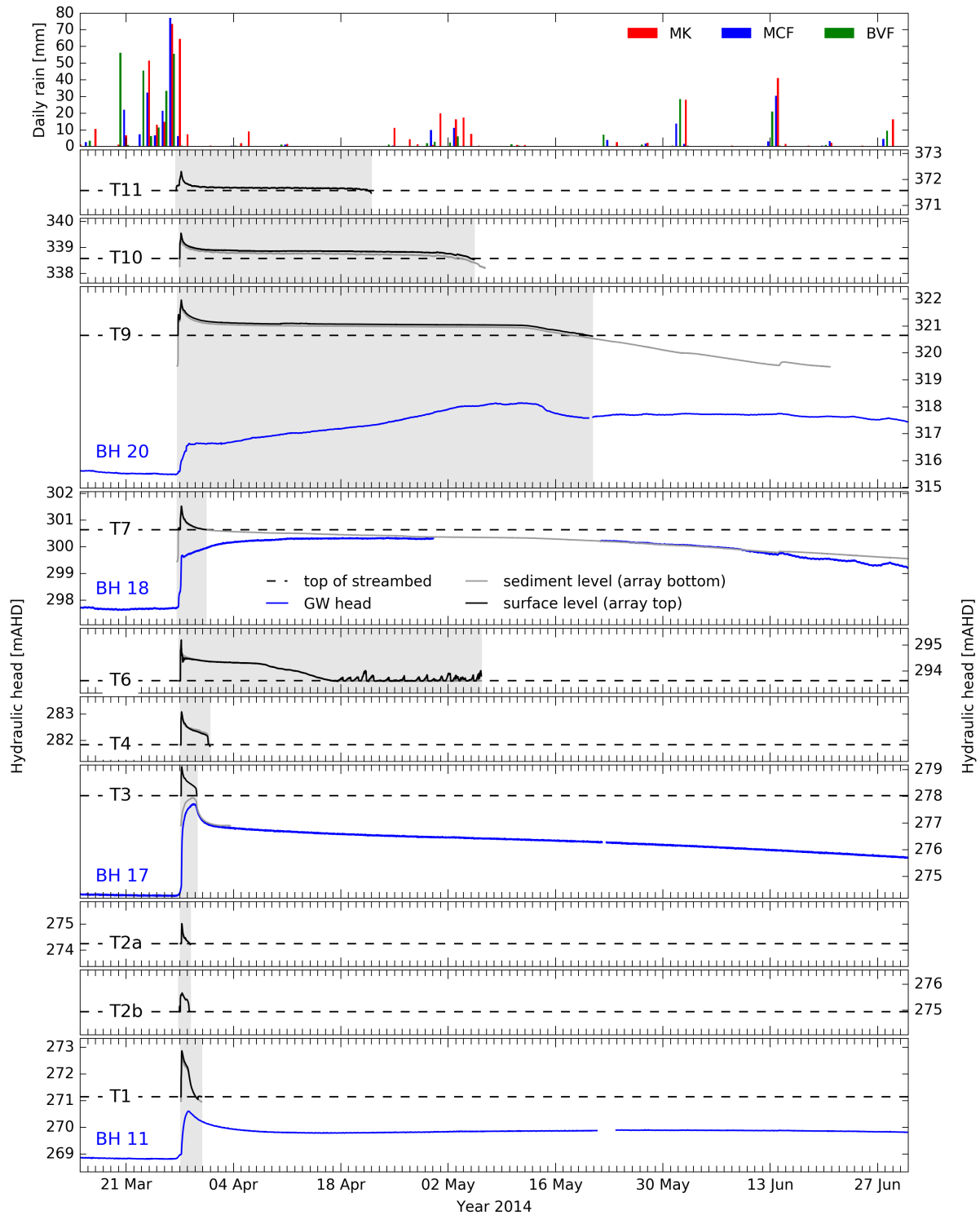


FIGURE 4: Daily rainfall recorded at three stations in the Maules Creek Catchment, hydraulic heads recorded by the streambed arrays installed along Middle Creek, including the nearby groundwater heads where available. Time periods when standing or flowing water was present at the streambed surface are highlighted in grey. Refer to Figure 2 for streambed array and borehole locations. Note that arrays T8 and T5 did not contain pressure transducers.

402 for arrays located at the upper end of the alluvium. During this time surface  
403 water was contained in the stream channel. A steady but significant decline  
404 in water level followed this period of stable water level.

405 The difference in surface flow behaviour is clearly depicted in Figure 4  
406 and is controlled by the rate of groundwater redistribution in the subsurface  
407 [7]. It is clear that much of the surface water is retained in the upper part of  
408 the channel (upstream from array T6, Figure 2) whereas the lower part of the  
409 creek shows short periods of surface run-off consistent with the behaviour of  
410 a disconnected ephemeral system [56, 6]. The cause of this behaviour is the  
411 subject of ongoing research beyond the scope of this paper, but it is likely  
412 controlled by the particle size distribution of the sediment and the general  
413 heterogeneity of the channel sediments [58, 20].

#### 414 3.4. *Thermal conditions at the streambed surface*

415 Figure 5 illustrates the temperature data recorded by the uppermost pres-  
416 sure transducer of each array (located at the streambed surface) in individual  
417 time colour bars for each location along the channel. Note that the uppermost  
418 logger in array T5 failed during deployment and this location is therefore ex-  
419 cluded from further analysis. The times when surface water was present, as  
420 indicated by the sensor measuring values above atmospheric pressure, are  
421 indicated as horizontal lines. The air temperature (MCF weather station), is  
422 plotted for comparison and varied between  $-0.7$  and  $33.5^{\circ}C$  while the sedi-  
423 ment surface temperatures varied between  $2.7$  and  $45.4^{\circ}C$ .

424 A decrease in overall temperature reflects the transition between autumn  
425 and winter in the southern hemisphere. While there is an obvious correlation  
426 between the air and the streambed surface temperature, the diel tempera-  
427 ture fluctuations are more pronounced at the streambed surface and vary  
428 depending on the array location. Thermal conditions at the streambed sur-  
429 face were affected by direct insolation during day time and differ depending  
430 on location settings caused by variable amounts of shading. The similarity of  
431 thermal conditions with low diel variability during the flow event is apparent.

432 The streambed surface temperatures clearly contain diel temperature os-  
433 cillations modulated by mesoscale weather events (Figure 5). Figure 6 shows  
434 the diel amplitudes extracted from the air and streambed surface tempera-  
435 ture records using *FFT* analysis. The range of air temperature amplitudes  
436 was between  $1.1$  and  $9.7^{\circ}C$ , whereas the range of streambed surface tem-  
437 perature amplitudes ranged between  $0$  and  $10^{\circ}C$ . A correlation between air  
438 and streambed surface temperature amplitudes is clearly visible in Figure 6

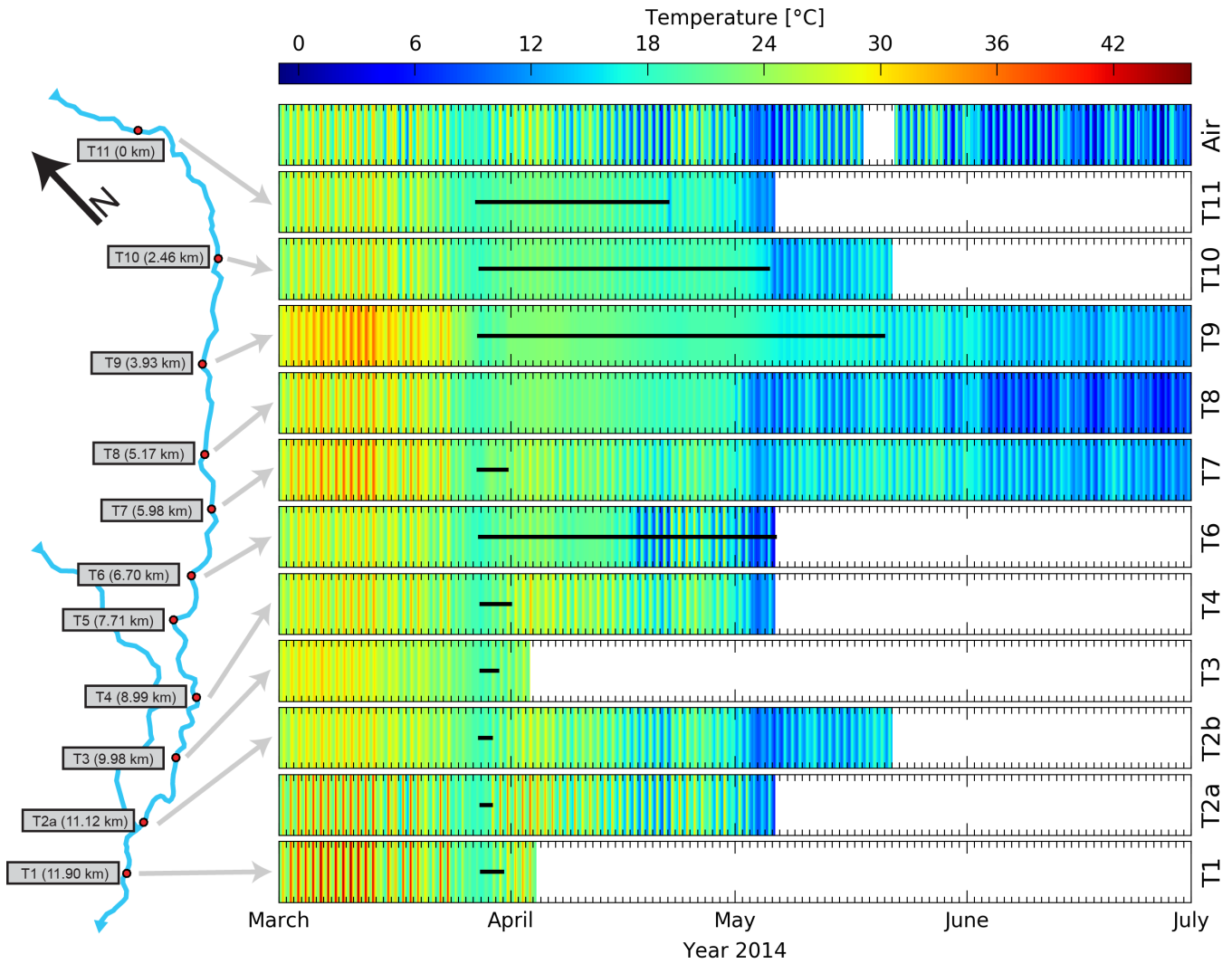


FIGURE 5: Temperatures recorded in the air and at the streambed surface along Middle Creek. Black lines indicate saturated conditions at the surface, i.e. the time during which the sensor was submerged in water. Note that the air temperature was not recorded during a small period in May 2014, that array T8 did not contain a pressure transducer, and that array T5 probe failed during deployment.

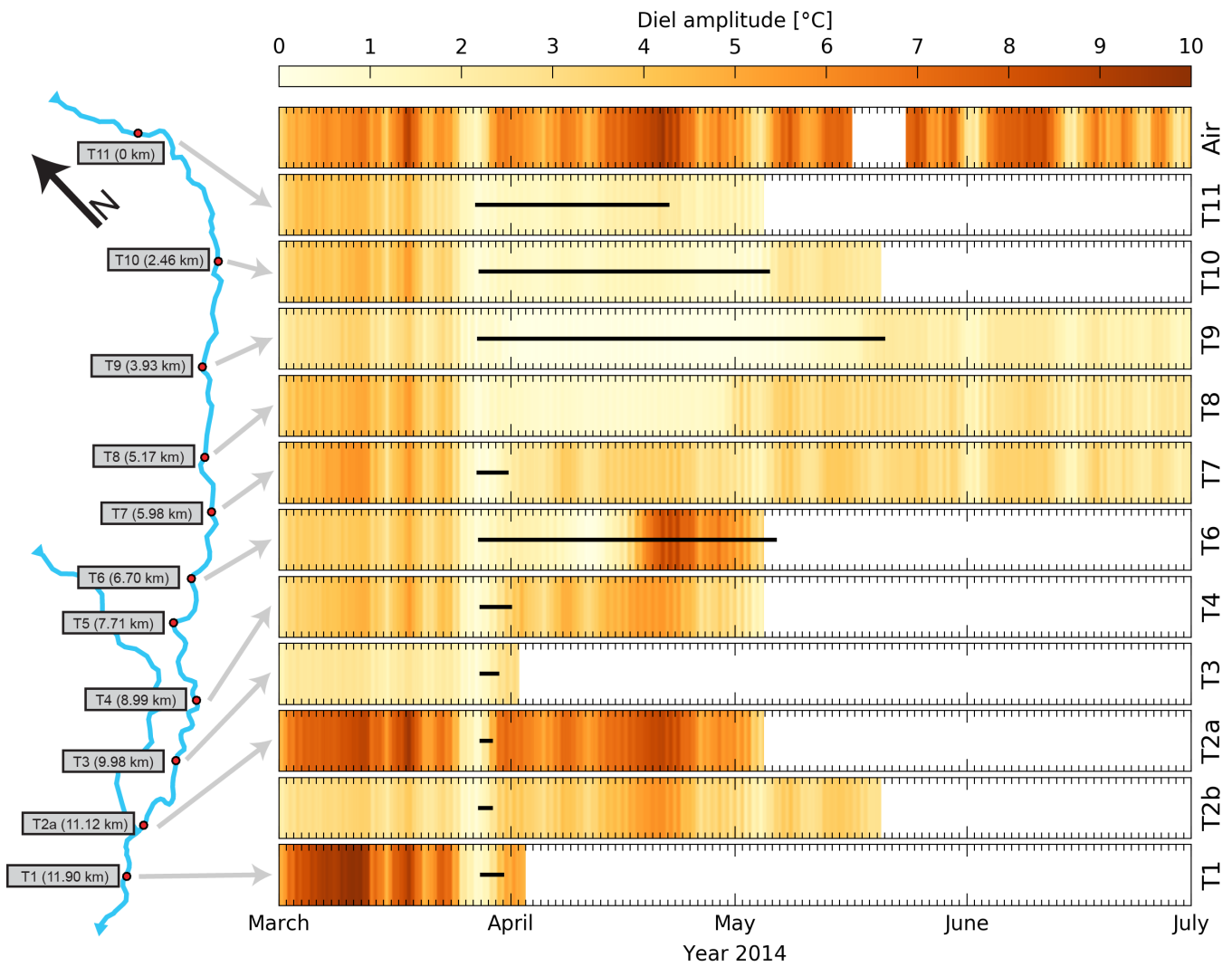


FIGURE 6: Amplitudes of the diel component of recorded temperature variations in the air and at the streambed surface along Middle Creek. Black lines indicate saturated conditions at the surface, i.e. the time during which the sensor was submerged in water.

439 for periods when the streambed surface was dry. Diel amplitudes show si-  
440 gnificant damping during the flow event when ponded or flowing water was  
441 present at the streambed sediment surface.

442 As observed by Constantz et al. [16], the onset of flow is preceded by lower  
443 absolute temperatures and smoothed diel amplitudes associated with the  
444 mesoscale low-pressure system. Our measurements confirm that flow cannot  
445 be deduced from temperature measurements and extracted amplitudes alone.

### 446 3.5. Streambed thermal signatures can detect the presence of water and cha- 447 racterise vertical water movement

448 If amplitude ratios for dry and saturated conditions can be calculated,  
449 then the vertical amplitude ratio time series in shallow streambed sediments  
450 (Figure 6) can be used to detect both the presence of water and to characte-  
451 rise the flow regimes according to the theory developed above. While  $A_r^{dry}$  can  
452 be evaluated from measurements during dry periods,  $A_r^{sat}$  requires estima-  
453 tion based on the likely values established from Monte-Carlo analysis. Note  
454 that the difference between both values is relatively small ( $\Delta A_r^{dry,sat} < 0.12$ ).  
455 Both values constrain a narrow range between them where the interpretation  
456 of vertical flow is ambiguous. However, as explained in Section 2.3,  $A_r$  values  
457 outside that range are directly indicative of the direction and magnitude of  
458 vertical water flow.

459 The amplitude ratio  $A_r^{dry}$  for dry streambed sediments at each location  
460 was calculated using the diel amplitudes extracted from temperature records  
461 using FFT analysis between 8-15 March 2014, and values are summarised in  
462 Table 2. While thermal diffusivity results comply with those calculated from  
463 the *Monte-Carlo* analysis, they are higher than expected which indicates the  
464 presence of large sized grains. Visual inspection of the streambed sediments  
465 confirms this inference and many large cobbles can be seen in the foreground  
466 of Figure 3 [41].

467 During flow events (wet streambed conditions) the amplitude ratio will  
468 depend on the vertical streambed water flux (see Equation 4). Theoretically,  
469 the  $A_r$  could be used to quantify this vertical flux [38, 59] and, provided that  
470 phases of the diel frequency components are also extracted, the saturated  
471 thermal diffusivity of the streambed could also be quantified [52, 60]. Howe-  
472 ver, Rau et al. [49] demonstrated that analytical heat tracing methods fail to  
473 provide accurate results when the diel component in the temperature signal  
474 is non-stationary. This includes highly transient infiltration as is expected

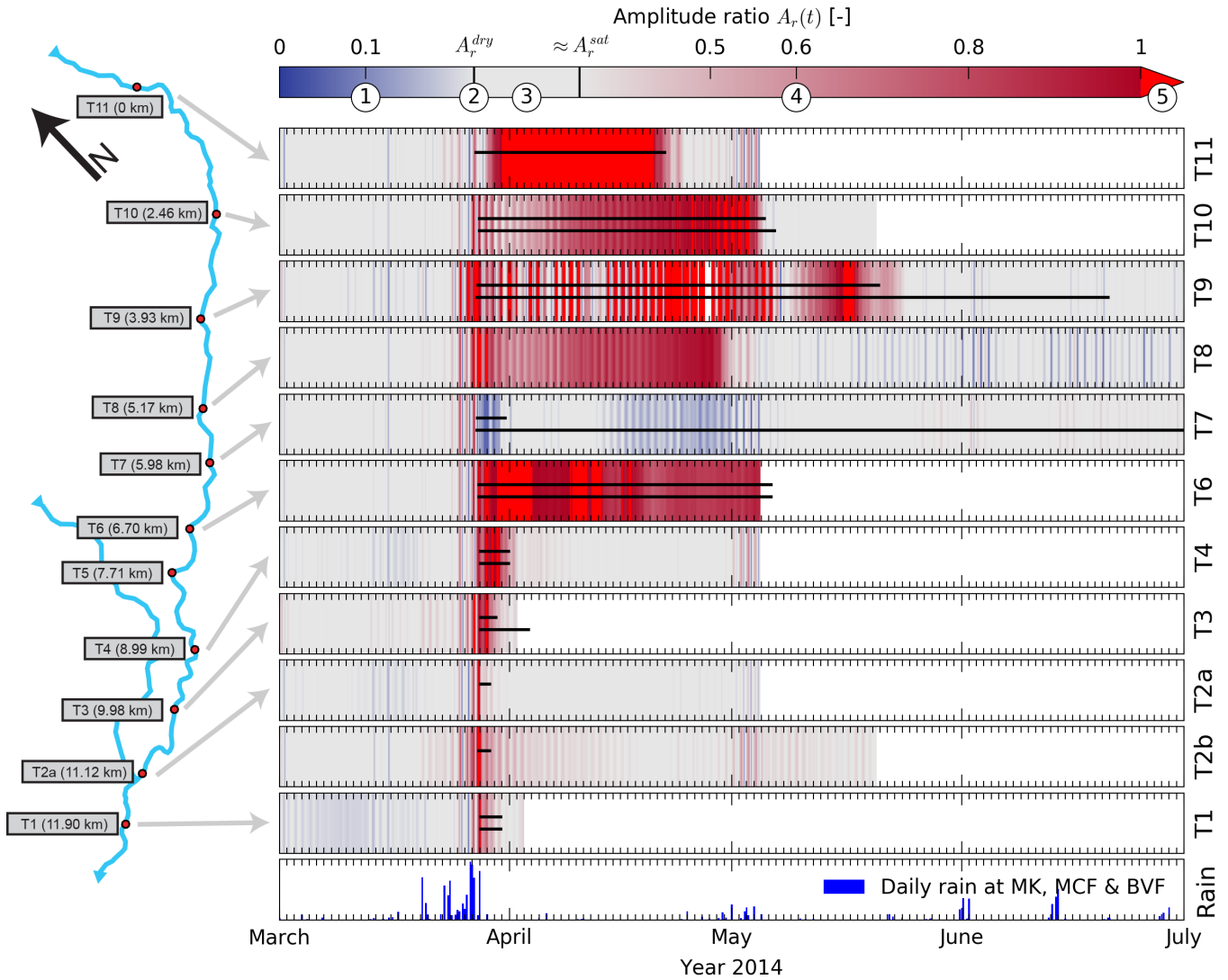


FIGURE 7: Diel temperature amplitude ratios  $A_r$  between the uppermost pair of sensors in the streambed. The colour map is adapted for each location to correctly reflect :  $A_r^{dry}$  as established from measurements during a dry period, and  $A_r^{sat} = A_r^{dry} + \Delta A_r$  calculated using thermal diffusivity values from *Monte-Carlo* results as well as site-specific sensor spacings. The colours reflect saturated conditions, where increasing blue represents an increasing vertical upward flow component (1) and colours increasing towards red represent increasing vertical downward flow component (4). Red reflects periods during which the  $A_r > 1$  and indicates horizontal hyporheic flow (5). Black lines indicate wet conditions at the surface (top) and at depth (bottom) in the streambed, i.e. the times during which the loggers were submerged in water. The numbers along the colour bar correspond to the thermal signature characterizations defined in Section 2.3 and Figure 1. The daily rain is plotted to show the influence on the streambed thermal regime.

475 during the dynamic flow events which are characteristic of Middle Creek  
476 (Figure 4). We therefore abstain from using phase results in our analysis.

477 Figure 7 shows the amplitude ratio time series for all arrays along Middle  
478 Creek translated into colours that reflect the different categories explained  
479 in Figure 1. It is clear that  $A_r$  can be used to distinguish between dry and  
480 saturated streambed conditions as confirmed by the pressure transducers de-  
481 tecting water (compare the black line with the coloured pattern representing  
482  $A_r$  variation). The influence of rainfall prior to the arrival of the surface  
483 run-off is also detected. Further, most arrays show variable downward water  
484 movement throughout the flow event (red colour corresponding to range 4 in  
485 Figure 1) as is expected for an intermittent system. The only exception is T7  
486 which indicates upward movement during the period of surface run-off and is  
487 discussed later. Here, water is retained within the alluvium for a time period  
488 that exceeds all other locations, as indicated by the hydrograph measured by  
489 the sensor at the bottom of the streambed array (Figures 4).

490 The results in Figure 7 contain a wealth of information that could be  
491 attributed to processes that have been found to influence transitory SW-GW  
492 interactions. For example, it is widely accepted that the hydraulic properties  
493 of alluvial sediments are strongly heterogeneous which can lead to zones of  
494 variable saturation beneath the stream [61, 62]. A field investigation using  
495 moisture sensors to measure the temporal behaviour of infiltration has repor-  
496 ted localised preferential flow which contributes to a rising water mound that  
497 can saturate the streambed from the bottom upwards [18]. An increase in  
498 saturation in the alluvial sediments due to infiltration may be considerably  
499 delayed after the onset of flow due to variability in sediment properties such  
500 as grain size [18, 63]. Moreover, certain combinations of channel geometry  
501 and stream water level can induce water saturation beneath the stream but  
502 without a saturated connection to the groundwater (inverted water table)  
503 [64].

504 We note that all these processes could affect the shallow streambed ther-  
505 mal diffusivity and therefore also the derived temperature amplitude ratios.  
506 As an example, T11 illustrates a thermal signature indicative of variably sa-  
507 turated sediment at the beginning of the flow event (Figure 7) during the  
508 same time as the pressure transducer clearly indicates the presence of sur-  
509 face water (Figure 4). This observation is in agreement with the previous  
510 findings of delayed saturation or rising water mound and illustrates that  
511 thermal signatures can enhance interpretation of the complexity of dryland  
512 SW-GW interactions, even more so when combined with water level measu-

513 rements. We further note that thermal signatures and water levels acquired  
514 during multiple flow events can be used to reveal the temporal dynamics of  
515 infiltration over longer time scales which could enhance the interpretation  
516 of transience in streambed conductance[65]. This could further improve our  
517 understanding of the complex water flow dynamics at the variably saturated  
518 stream-aquifer interface.

### 519 3.6. Streambed thermal regimes and spatio-temporal flow behaviour

520 To characterise the thermal conditions during flow events, the hydraulic  
521 head and temperature records for two representative multi-level arrays were  
522 plotted for T9 in Figure 8 and for T7 in Figure 9. These plots include the  
523 temperature data measured at multiple levels within the topmost meter of  
524 the channel sediment and diel temperature amplitudes as extracted from  
525 the measurements using *FFT* analysis. Both streambed arrays contain the  
526 thermal signatures which are found in all other locations (Figure 7) and are  
527 therefore worthy of detailed inspection.

528 Figure 8a clearly shows the temporal character of flow events measured  
529 at the location of streambed array T9. T7 shows a similar hydrograph mea-  
530 sured by the pressure transducer at the bottom, but the one at the top only  
531 captured the peak of the flow event whereas the bottom logger remained  
532 submerged in water contained in the streambed for a period of time. From  
533 Figure 4 it is clear that all hydrographs which captured more than the initial  
534 peak illustrate a similar shape but with differing duration of the stable or  
535 receding water level (intermittent stream behaviour).

536 The following flow regimes can be derived from the observed hydrograph  
537 shapes, and are categorised below and illustrated in a conceptual model of  
538 transitory surface-groundwater interactions (Figure 10, colours refer to Fi-  
539 gures 8 and 9) :

540 [A] Dry channel (red) as a default for dryland streams : The dry sediments  
541 are characterised by large temperature amplitudes at the surface that  
542 is rapidly damped with depth for both T9 (Figure 8b) and T7 (Figure  
543 9b). The large amplitudes at the boundary are a result of insolation and  
544 indicate dry conditions (absence of water). The  $A_r$ -depth profile for a  
545 location, as shown in Figures 8d and 9d, can be used to benchmark the  
546 thermal conditions in the dry streambed.

547 [B] Rapid surface run-off (green) : Surface run-off and infiltration along the  
548 channel may result in a spatially heterogeneous distribution of alluvium

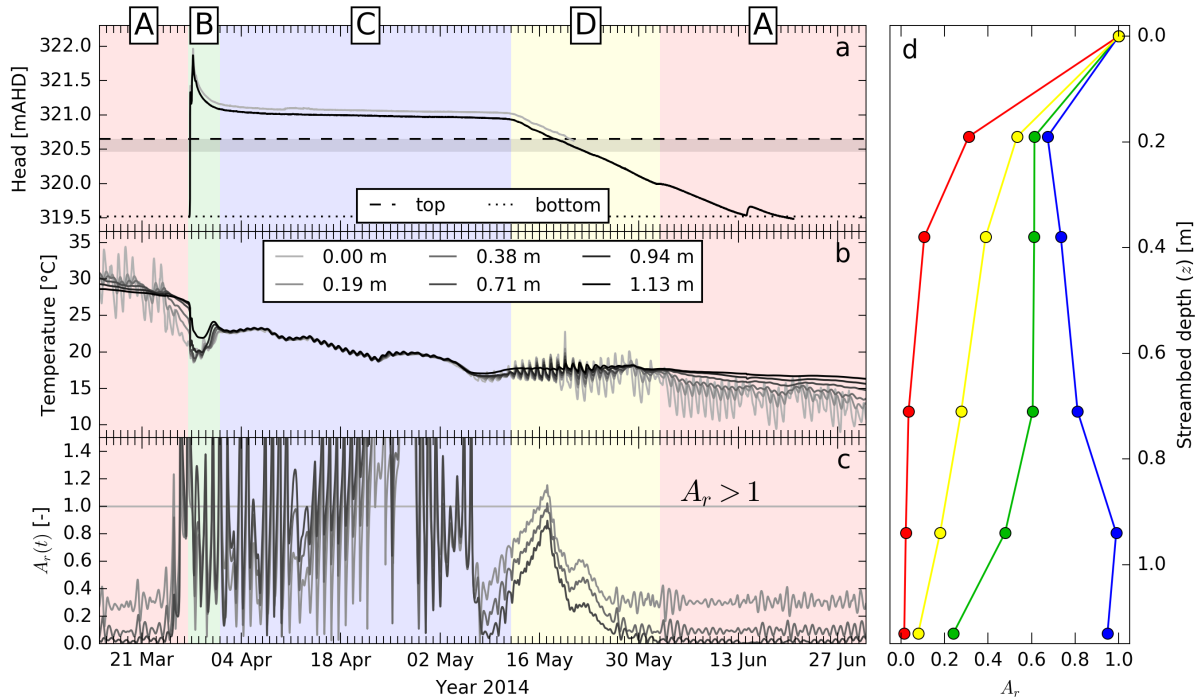


FIGURE 8: Streambed array T9 : a) Hydraulic head at the top and bottom of the array. The grey band indicates the depth interval in which temperature data is interpreted in Figure 7. b) Multi-level temperature records. b) Multi-level temperature records. c) Amplitude ratio time series  $A_r(t)$  of the diel temperature component for 3 depths (same legend as panel b). d) Depth profiles of diel temperature amplitude ratios averaged over the time period corresponding to the colour coded flow regimes  $A$ - $D$  labelled at the top of panel (a) and which are sketched in Figure 10

549 water saturation beneath the channel. Upon arrival of the water in the  
 550 dry channel, the temperature rapidly changes over depth with an asso-  
 551 ciated increase in the diel temperature amplitude (Figures 8b and 9b).  
 552 This reflects the highly transient infiltration of water which carries a  
 553 contrasting temperature downwards [24]. Further, this marks a period  
 554 of highly transient infiltration [29, 66] in particular for locations that  
 555 show ephemeral behaviour (T4-T1 in Figure 7). The streambed satu-  
 556 ration may be significantly delayed compared to the arrival of surface  
 557 water (T11 in Figure 7).

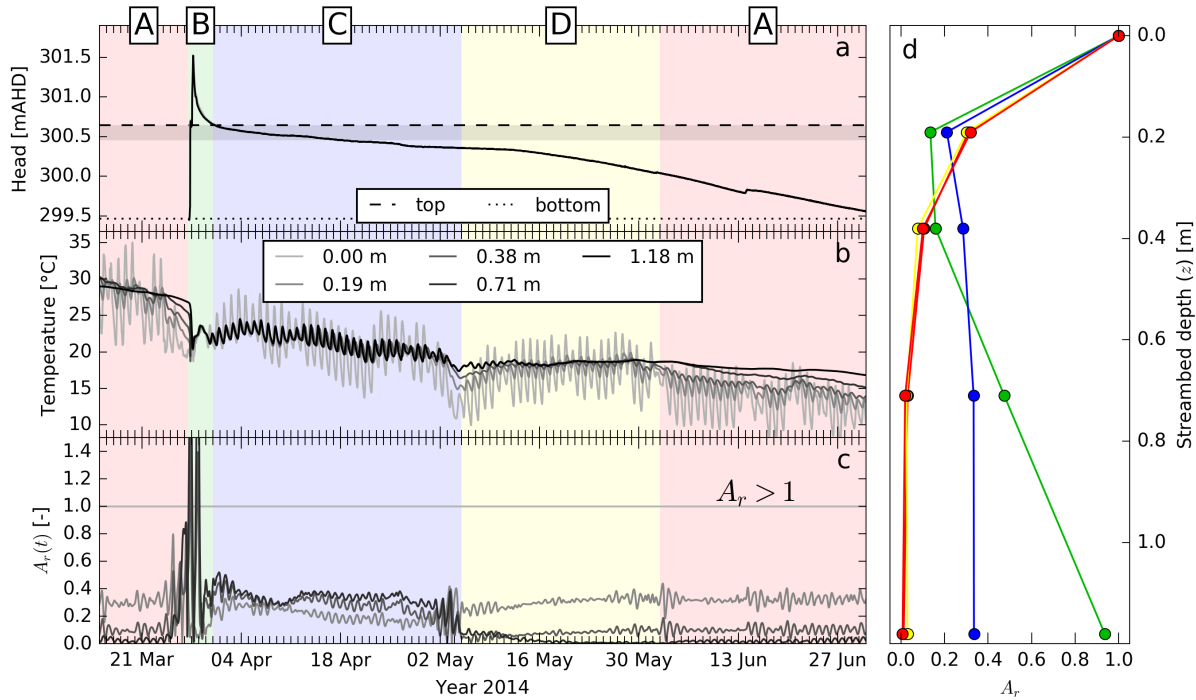


FIGURE 9: Streambed array T7 : a) Hydraulic head at the top and bottom of the array. The grey band indicates the depth interval in which temperature data is interpreted in Figure 7. b) Multi-level temperature records. c) Amplitude ratio time series  $A_r(t)$  of the diel temperature component for 3 depths (same legend as panel b). d) Depth profiles of diel temperature amplitude ratios averaged over the time period corresponding to the colour coded flow regimes A-D labelled at the top of panel (a) and which are sketched in Figure 10

558 [C] Pool-riffle sequence (blue) : This regime is characterised by water flow  
 559 through pool-riffle sequences including varying proportions of both sub-  
 560 surface (hyporheic) and surface flow that is predominantly horizontal.  
 561 It only occurs if the infiltrated water is not redistributed fast enough  
 562 so that the groundwater table rises above the streambed surface there-  
 563 by intersecting the channel topography. The duration of this regime  
 564 varies depending on the lateral aquifer response time (ART), the rate  
 565 at which the subsurface water mound redistributes [7]. Consequently,  
 566 this regime is much shorter or may never be reached in locations that  
 567 have a low ART. Further, the timing of the transition to the next flow

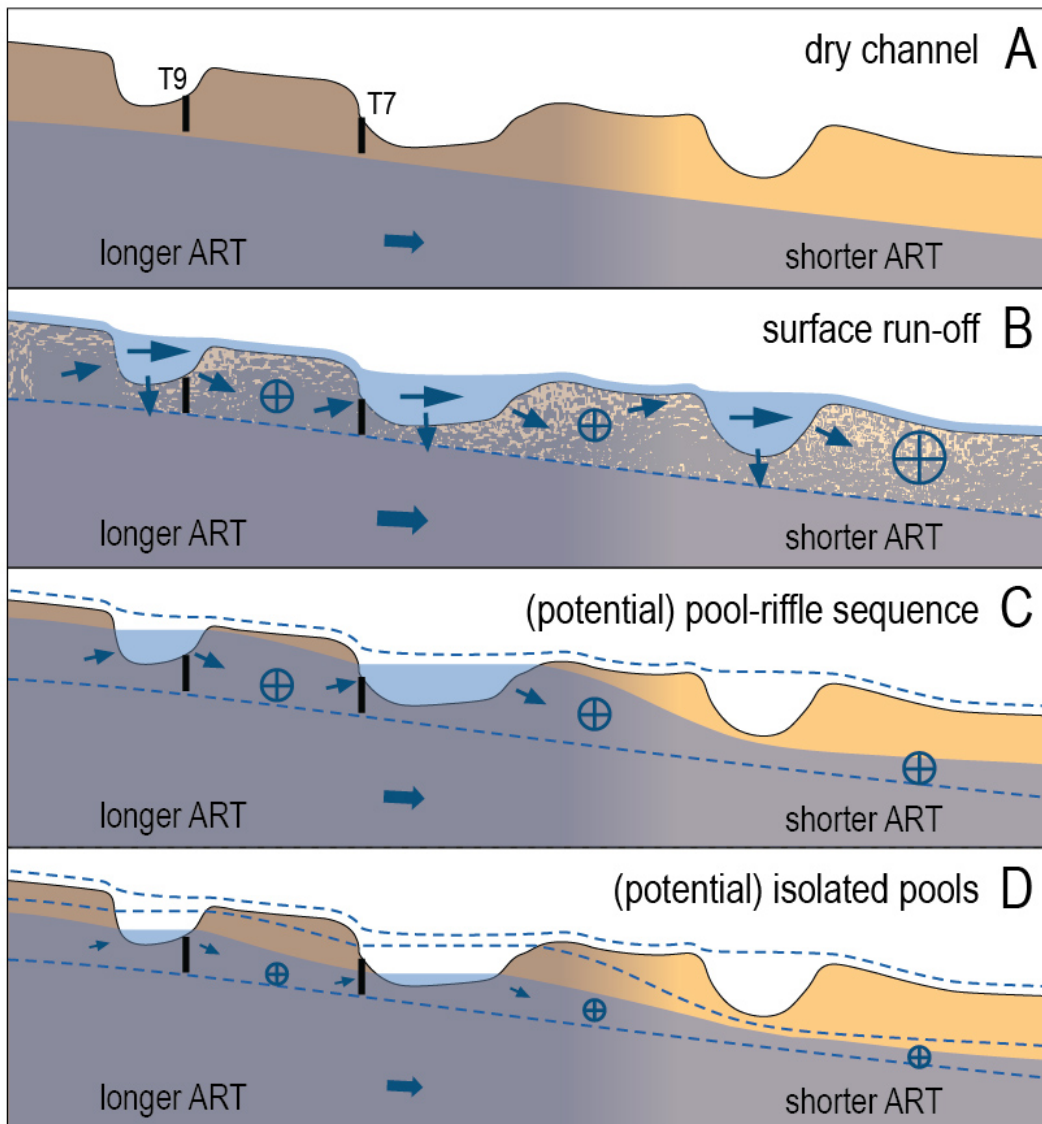


FIGURE 10: Conceptual model of the different hydrological regimes that occur during transitory surface water-groundwater interactions in ephemeral or intermittent streams. Note that while the regions of longer and shorter aquifer response time (ART, a measure for the redistribution rate of infiltrated water [7]) greatly simplify realistic conditions, it is reflective of our field conditions and provides a range of conditions which may be relevant to other studies. A variable ART also explains the potential occurrence of regime C and D. Note further that streambed arrays T9 and T7 are located to qualitatively reflect the measured water levels and thermal signatures (Figures 8 and 9). The hydrological and thermal conditions of this sequence is detailed in the discussion.

568 regime depends on the local streambed morphology and is therefore so-  
569 mewhat ambiguous. The shallow subsurface temperatures during this  
570 regime are similar to those observed in perennial systems dominated  
571 by hyporheic exchange [67, 68].

572 During this flow regime, the locations show differing behaviour : T9 fea-  
573 tures an  $A_r$ -depth profile that is significantly different from dry condi-  
574 tions and indicates a downward flow component (Figure 8). In contrast,  
575 the shallower part of T7 indicates an upward flow component whereas  
576 the deeper part shows increasingly downward flow (Figure 9). The dif-  
577 ference between T9 and T7 are indicative of their different locations  
578 within the pool-riffle sequence and in relative elevation of water table  
579 relative to the ground surface (Figure 10). T7 was located at the end  
580 of a gravel bar with up-welling hyporheic flow at the top of the array  
581 throughout the short duration of the surface run-off. T9 was located at  
582 the downstream end of a pool.

583 Note that the array locations relative to the pool-riffle system will  
584 change as the water level recedes, and also due to potential erosion  
585 during surface run-off. It is noteworthy that during this flow regime  
586 the diel amplitude propagates to the lowest sensor in the sediment and  
587 can cause an amplitude ratio that is larger than unity ( $A_r > 1$ ) thus vio-  
588 lating the conditions required to apply vertical analytical heat tracing.  
589 In the absence of a subsurface thermal source,  $A_r > 1$  is an indicator  
590 for hyporheic flow with a significant horizontal component [47, 69].

591 [D] Cessation of riffle flow and drying of the isolated pools and sediments  
592 (yellow) : A steady decrease in hydraulic head indicates that water  
593 is redistributing in the subsurface leaving the channel sediments to  
594 dry out. Similar to (C), this regime may be bypassed under certain  
595 conditions. The increase of the diel temperature amplitude, particularly  
596 at the lower sensors, is an indication of a significant downward water  
597 flux.

598 Our conceptual model is supported by the fact that surface flow exists at  
599 locations when surface water further upstream has disappeared (Figure 4).  
600 Consequently, water contained in the shallow alluvium must move down-  
601 stream and sideways as the overall water table elevation slowly falls below the  
602 lowest elevations of the streambed surface. We further note that the existence  
603 of these regimes was verified by visual observations made during numerous  
604 field trips throughout the hydrological sequence. This is further verified by

605 time lapse images captured using a camera mounted beside the stream near  
606 BH20/T9, as described in a previous study [7].

#### 607 4. Conclusions

608 We have shown how amplitude ratios of the diel component in tempera-  
609 ture time series measured at two vertical locations in shallow streambeds can  
610 be used to detect saturation conditions and to characterise transitory flow  
611 conditions. This is an advantage over head measurements due to the lower  
612 cost involved and ease of installation which allows the possibility of a wider  
613 spatial deployment of sensors. Amplitude ratios depend on the sediment ther-  
614 mal diffusivity, which is a function of the different thermal properties of air or  
615 water occupying the pore space. While the dry streambed thermal diffusivity  
616 can be determined from temperature records acquired during dry periods,  
617 the saturated thermal diffusivity is always higher depending on the sediment  
618 properties. The likely difference between dry and saturated amplitude ra-  
619 tios does not exceed  $\sim 0.175$  as illustrated using a *Monte-Carlo* analysis with  
620 probable ranges in matrix thermal properties available in the literature.

621 A small range of amplitude ratios exists for which interpretation of the  
622 state of saturation is ambiguous, i.e. either variably saturated sediments or  
623 full saturation with upward flow. The range of ambiguity is determined by the  
624 difference between dry and saturated streambed thermal diffusivity, which  
625 depends both on porosity and matrix thermal properties. However, when  
626 interpreted in combination with pressure data, which is indicative of whether  
627 or not water is present above the point of measurement, this range can still  
628 be used to reveal streambed processes.

629 We have applied this new approach to multi-level temperature data from  
630 streambed arrays deployed along a  $\sim 12$  km channel section. Hydraulic heads  
631 were measured simultaneously by the arrays as well as at co-located shallow  
632 piezometers. The data demonstrate that intermittent surface water-groundwater  
633 interactions are highly variable in space and time. The interpreted tempera-  
634 ture and pressure data enable categorization of these interactions into four  
635 generic hydrological regimes that can occur sequentially in time : (A) dry  
636 channel, (B) rapid surface run-off along the channel, (C) pool-riffle sequence  
637 with horizontal hyporheic flow, (D) isolated pools. The duration of each re-  
638 gime will depend on the channel morphology as well as the lateral aquifer  
639 response time (ART) which controls the rate of groundwater redistribution.  
640 Our results illustrate that sequence C and D may not be reached in the case

641 that the infiltrated water is redistributed fast enough so that the groundwater  
642 level does not rise above the streambed surface for a significant duration.

643 Such analysis enables determination of the intricate dynamics inherent to  
644 the connectivity between intermittent surface flow and groundwater and is  
645 directly relevant to other semi-arid and arid regions of the world [1]. Unders-  
646 tanding such hydrological behaviour is imperative to conjunctive resource  
647 management in water-limited environments [2]. Furthermore, thermal condi-  
648 tions in the shallow streambed influence water quality through hydrochemical  
649 and biological processing and determine the ecological habitat [70, 1]. Our  
650 approach to monitoring, understanding and interpreting thermal regimes in  
651 intermittent and ephemeral streams can, therefore, improve spatiotemporal  
652 understandings of hyporheic processes and associated water quality dyna-  
653 mics, groundwater recharge, and when and how dryland streams support  
654 riparian ecosystems.

## 655 **Acknowledgements**

656 We are grateful for technical and field support provided by Evan Jensen, Ed-  
657 wina Davison, Calvin Li and to landowners in Mauls Creek (Philip Laird, Alistair  
658 Todd, and Steve Bradshaw) for giving access to the field sites. The figures in this  
659 manuscript were made with the help of *Matplotlib* [71]. The data used in this ana-  
660 lysis was collected with equipment provided by the Australian Federal Government  
661 financed *National Collaborative Research Infrastructure Scheme (NCRIS)*, data  
662 available at : <http://groundwater.anu.edu.au/fieldsite/maules-creek>). We  
663 would like to thank the Cotton Catchment Communities CRC for their financial  
664 support (Cotton CRC projects 2.02.03 and 2.02.21). The elevation data in Figure 2  
665 is courtesy of *Geoscience Australia* <http://www.ga.gov.au>. MOC was suppor-  
666 ted by the European Community’s Seventh Framework Program (FP7/2007-2013)  
667 under grant agreement 299091. GCR was supported by the *National Centre for*  
668 *Groundwater Research and Training (NCGRT)*, an Australian Government ini-  
669 tiative supported by the *Australian Research Council (ARC)* and the *National*  
670 *Water Commission (NWC)*. LJSH was supported by the NSW State Govern-  
671 ment’s *Research Acceleration and Attraction Program (RAAP)* in the year 2016.  
672 We further thank the Editor Paolo D’Odorico as well as the AE and 2 reviewers (all  
673 anonymous) for handling and suggesting improvements to this manuscript during  
674 peer-review.

675 **References**

- 676 [1] T. Datry, K. Fritz, C. Leigh, Challenges, developments and perspectives  
677 in intermittent river ecology, *Freshwater Biology* (2016) 1171–1180.
- 678 [2] L. R. Levick, D. C. Goodrich, M. Hernandez, J. Fonseca, D. J. Sem-  
679 mens, J. Stromberg, M. Tluczek, R. a. Leidy, M. Scianni, P. D. Guertin,  
680 W. G. Kepner, The Ecological and Hydrological Significance of Ephe-  
681 meral and Intermittent Streams in the Arid and Semi-arid American  
682 Southwest, Technical Report, US Environmental Protection Agency and  
683 USDA/ARS So, 2008.
- 684 [3] J. Constantz, C. L. Thomas, G. Zellweger, Influence of diurnal variations  
685 in stream temperature on streamflow loss and groundwater recharge,  
686 *Water Resources Research* 30 (1994) 3253–3264.
- 687 [4] J. Lange, Dynamics of transmission losses in a large arid stream channel,  
688 *Journal of Hydrology* 306 (2005) 112–126.
- 689 [5] B. R. Scanlon, K. E. Keese, A. L. Flint, L. E. Flint, C. B. Gaye, W. M.  
690 Edmunds, I. Simmers, Global synthesis of groundwater recharge in se-  
691 miarid and arid regions, *Hydrological Processes* 20 (2006) 3335–3370.
- 692 [6] M. Shanafield, P. G. Cook, Transmission losses, infiltration and ground-  
693 water recharge through ephemeral and intermittent streambeds : A re-  
694 view of applied methods, *Journal of Hydrology* 511 (2014) 518–529.
- 695 [7] M. O. Cuthbert, R. I. Acworth, M. S. Andersen, J. R. Larsen, A. M.  
696 McCallum, G. C. Rau, J. H. Tellam, Understanding and quantifying  
697 focused, indirect groundwater recharge from ephemeral streams using  
698 water table fluctuations, *Water Resources Research* 52 (2016) 827–840.
- 699 [8] T. R. Labbe, K. D. Fausch, Dynamics of intermittent stream habitat  
700 regulate persistence of a threatened fish at multiple scales, *Ecological*  
701 *Applications* 10 (2000) 1774–1791.
- 702 [9] I. Simmers, *Understanding Water in a Dry Environment - hydrological*  
703 *processes in arid and semi-arid zones*, volume 23, Taylor & Francis, 2003.

- 704 [10] R. G. Taylor, M. C. Todd, L. Kongola, L. Maurice, E. Nahozya,  
705 H. Sanga, A. M. MacDonald, Evidence of the dependence of groundwa-  
706 ter resources on extreme rainfall in East Africa, *Nature Climate Change*  
707 3 (2012) 374–378.
- 708 [11] M. O. Cuthbert, G. M. Ashley, A Spring Forward for Hominin Evolution  
709 in East Africa, *PLoS ONE* 9 (2014) e107358.
- 710 [12] Y. Wada, L. P. H. Van Beek, C. M. Van Kempen, J. W. T. M. Reckman,  
711 S. Vasak, M. F. P. Bierkens, Global depletion of groundwater resources,  
712 *Geophysical Research Letters* 37 (2010) L20402.
- 713 [13] T. Gleeson, W. M. Alley, D. M. Allen, M. A. Sophocleous, Y. Zhou,  
714 M. Taniguchi, J. Vandersteen, Towards sustainable groundwater use :  
715 Setting long-term goals, backcasting, and managing adaptively, *Ground*  
716 *Water* 50 (2012) 19–26.
- 717 [14] Y. Wada, L. P. H. van Beek, N. Wanders, M. F. P. Bierkens, Human  
718 water consumption intensifies hydrological drought worldwide, *Environ-*  
719 *mental Research Letters* 8 (2013) 034036.
- 720 [15] J. Constantz, C. L. Thomas, The Use of Streambed Temperature Pro-  
721 files to Estimate the Depth, Duration, and Rate of Percolation Beneath  
722 Arroyos, *Water Resources Research* 32 (1996) 3597–3602.
- 723 [16] J. Constantz, D. Stonestrom, A. E. Stewart, R. Niswonger, T. R. Smith,  
724 Analysis of streambed temperatures in ephemeral channels to determine  
725 streamflow frequency and duration, *Water Resources Research* 37 (2001)  
726 317–328.
- 727 [17] W. B. Bull, Discontinuous ephemeral streams, *Geomorphology* 19 (1997)  
728 227–276.
- 729 [18] O. Dahan, B. Tatarsky, Y. Enzel, C. Kulls, M. Seely, G. Benito, Dyna-  
730 mics of flood water infiltration and ground water recharge in hyperarid  
731 desert, *Ground Water* 46 (2008) 450–461.
- 732 [19] P. Brunner, C. T. Simmons, P. G. Cook, Spatial and temporal aspects  
733 of the transition from connection to disconnection between rivers, lakes  
734 and groundwater, *Journal of Hydrology* 376 (2009) 159–169.

- 735 [20] D. J. Irvine, P. Brunner, H.-J. H. Franssen, C. T. Simmons, Hetero-  
736 geneous or homogeneous? Implications of simplifying heterogeneous  
737 streambeds in models of losing streams, *Journal of Hydrology* 424-425  
738 (2012) 16–23.
- 739 [21] J. Constantz, Interaction between stream temperature, streamflow, and  
740 groundwater exchanges in alpine streams, *Water Resources Research* 34  
741 (1998) 1609–1615.
- 742 [22] J. Constantz, C. L. Thomas, Stream bed temperature profiles as indi-  
743 cators of percolation characteristics beneath arroyos in the Middle Rio  
744 Grande Basin, USA, *Hydrological Processes* 11 (1997) 1621–1634.
- 745 [23] K. W. Blasch, T. P. a. Ferré, J. P. Hoffmann, A Statistical Technique  
746 for Interpreting Streamflow Timing Using Streambed Sediment Ther-  
747 mographs, *Vadose Zone Journal* 3 (2004) 936.
- 748 [24] J. Constantz, A. Stewart, R. Niswonger, L. Sarma, Analysis of tempera-  
749 ture profiles for investigating stream losses beneath ephemeral channels,  
750 *Water Resources Research* 38 (2002) 1–13.
- 751 [25] B. K. W. Blasch, J. Constantz, D. A. Stonestrom, Thermal Methods for  
752 Investigating Ground-water Recharge, Technical Report, 2007.
- 753 [26] M. P. Anderson, Heat as a Ground Water Tracer, *Ground Water* 43  
754 (2005) 951–968.
- 755 [27] J. Constantz, Heat as a tracer to determine streambed water exchanges,  
756 *Water Resources Research* 44 (2008) n/a–n/a.
- 757 [28] G. C. Rau, M. S. Andersen, A. M. McCallum, H. Roshan, R. I. Acworth,  
758 Heat as a tracer to quantify water flow in near-surface sediments, *Earth-  
759 Science Reviews* 129 (2014) 40–58.
- 760 [29] K. W. Blasch, T. P. A. Ferré, J. P. Hoffmann, J. B. Fleming, Relative  
761 contributions of transient and steady state infiltration during ephemeral  
762 streamflow, *Water Resources Research* 42 (2006) W08405.
- 763 [30] L. J. Halloran, H. Roshan, G. C. Rau, M. S. Andersen, Calculating  
764 water saturation from passive temperature measurements in near-surface  
765 sediments : Development of a semi-analytical model, *Advances in Water  
766 Resources* 89 (2016) 67–79.

- 767 [31] L. J. S. Halloran, G. C. Rau, M. S. Andersen, Heat as a tracer to quantify  
768 processes and properties in the vadose zone : A review, *Earth-Science*  
769 *Reviews* 159 (2016) 358–373.
- 770 [32] H. S. Carslaw, J. C. Jaeger, *Conduction of heat in solids*, 1959.
- 771 [33] R. W. Stallman, Steady one-dimensional fluid flow in a semi-infinite  
772 porous medium with sinusoidal surface temperature, *Journal of Geo-*  
773 *physical Research* 70 (1965) 2821.
- 774 [34] S. Goto, Thermal response of sediment with vertical fluid flow to periodic  
775 temperature variation at the surface, *Journal of Geophysical Research*  
776 110 (2005) B01106.
- 777 [35] G. De Marsily, *Quantitative hydrogeology; groundwater hydrology for*  
778 *engineers*, Academic Press, New York, NY, USA, 1986.
- 779 [36] D. W. Waples, J. S. Waples, A Review and Evaluation of Specific Heat  
780 Capacities of Rocks, Minerals, and Subsurface Fluids. Part 1 : Minerals  
781 and Nonporous Rocks, *Natural Resources Research* 13 (2004) 97–122.
- 782 [37] G. C. Rau, M. S. Andersen, R. I. Acworth, Experimental investigation of  
783 the thermal dispersivity term and its significance in the heat transport  
784 equation for flow in sediments, *Water Resources Research* 48 (2012)  
785 n/a–n/a.
- 786 [38] C. E. Hatch, A. T. Fisher, J. S. Revenaugh, J. Constantz, C. Ruehl,  
787 Quantifying surface water-groundwater interactions using time series  
788 analysis of streambed thermal records : Method development, *Water*  
789 *Resources Research* 42 (2006) n/a–n/a.
- 790 [39] M. O. Cuthbert, R. MacKay, Impacts of nonuniform flow on estimates  
791 of vertical streambed flux, *Water Resources Research* 49 (2013) 19–28.
- 792 [40] M. O. Cuthbert, An improved time series approach for estimating  
793 groundwater recharge from groundwater level fluctuations, *Water Re-*  
794 *sources Research* 46 (2010) n/a–n/a.
- 795 [41] J. Côté, J.-M. Konrad, A generalized thermal conductivity model for  
796 soils and construction materials, *Canadian Geotechnical Journal* 42  
797 (2005) 443–458.

- 798 [42] Y. Dong, J. S. McCartney, N. Lu, Critical Review of Thermal Conduc-  
799 tivity Models for Unsaturated Soils, *Geotechnical and Geological Engi-  
800 neering* 33 (2015) 207–221.
- 801 [43] O. Johansen, *Thermal Conductivity of Soils*, Ph.D. thesis, University of  
802 Trondheim, 1975.
- 803 [44] W. Woodside, J. H. Messmer, *Thermal Conductivity of Porous Media.*  
804 *I. Unconsolidated Sands*, *Journal of Applied Physics* 32 (1961) 1688.
- 805 [45] NIST, *Chemistry WebBook*, 2017.
- 806 [46] C. Clauser, *Heat Transport Processes in the Earths Crust*, *Surveys in  
807 Geophysics* 30 (2009) 163–191.
- 808 [47] G. C. Rau, M. S. Andersen, A. M. McCallum, R. I. Acworth, Ana-  
809 lytical methods that use natural heat as a tracer to quantify surface  
810 groundwater exchange, evaluated using field temperature records,  
811 *Hydrogeology Journal* 18 (2010) 1093–1110.
- 812 [48] T. C. Winter, J. W. Harvey, O. L. Franke, W. M. Alley, *Ground wa-  
813 ter and surface water : a single resource*, Technical Report 1139, U.S.  
814 Geological Survey, 1998.
- 815 [49] G. C. Rau, M. O. Cuthbert, A. M. McCallum, L. J. S. Halloran, M. S.  
816 Andersen, Assessing the accuracy of 1-D analytical heat tracing for es-  
817 timating near-surface sediment thermal diffusivity and water flux under  
818 transient conditions, *Journal of Geophysical Research F : Earth Surface*  
819 120 (2015) 1551–1573.
- 820 [50] M. S. Andersen, R. I. Acworth, *Stream-aquifer interactions in the  
821 Maules Creek catchment, Namoi Valley, New South Wales, Australia*,  
822 *Hydrogeology Journal* 17 (2009) 2005–2021.
- 823 [51] B. M. S. Giambastiani, A. M. McCallum, M. S. Andersen, B. F. J.  
824 Kelly, R. I. Acworth, Understanding groundwater processes by repre-  
825 senting aquifer heterogeneity in the Maules Creek catchment, Namoi  
826 Valley (New South Wales, Australia), *Hydrogeology Journal* 20 (2012)  
827 1027–1044.

- 828 [52] A. M. McCallum, M. S. Andersen, G. C. Rau, R. I. Acworth, A 1-D  
829 analytical method for estimating surface water-groundwater interactions  
830 and effective thermal diffusivity using temperature time series, *Water*  
831 *Resources Research* 48 (2012).
- 832 [53] B. F. J. Kelly, W. A. Timms, M. S. Andersen, A. M. McCallum, R. S.  
833 Blakers, R. Smith, G. C. Rau, A. Badenhop, K. Ludowici, R. I. Acworth,  
834 Aquifer heterogeneity and response time : the challenge for groundwater  
835 management, *Crop and Pasture Science* 64 (2013) 1141–1154.
- 836 [54] A. M. McCallum, M. S. Andersen, G. C. Rau, J. R. Larsen, R. I. Ac-  
837 worth, River-aquifer interactions in a semiarid environment investiga-  
838 ted using point and reach measurements, *Water Resources Research* 50  
839 (2014) 2815–2829.
- 840 [55] M. B. Cardenas, Thermal skin effect of pipes in streambeds and its  
841 implications on groundwater flux estimation using diurnal temperature  
842 signals, *Water Resources Research* 46 (2010).
- 843 [56] P. Brunner, P. G. Cook, C. T. Simmons, Disconnected surface water  
844 and groundwater : From theory to practice, *Ground Water* 49 (2011)  
845 460–467.
- 846 [57] M. Shanafield, P. G. Cook, P. Brunner, J. Mccallum, C. T. Simmons,  
847 Aquifer response to surface water transience in disconnected streams,  
848 *Water Resources Research* 48 (2012) W11510.
- 849 [58] P. Brunner, P. G. Cook, C. T. Simmons, Hydrogeologic controls on  
850 disconnection between surface water and groundwater, *Water Resources*  
851 *Research* 45 (2009) W01422.
- 852 [59] J. Keery, A. Binley, N. Crook, J. W. Smith, Temporal and spatial varia-  
853 bility of groundwatersurface water fluxes : Development and application  
854 of an analytical method using temperature time series, *Journal of Hy-*  
855 *drology* 336 (2007) 1–16.
- 856 [60] C. H. Luce, D. Tonina, F. Gariglio, R. Applebee, Solutions for the diur-  
857 nally forced advection-diffusion equation to estimate bulk fluid velocity  
858 and diffusivity in streambeds from temperature time series, *Water Re-*  
859 *sources Research* 49 (2013) 488–506.

- 860 [61] J. H. Fleckenstein, R. G. Niswonger, G. E. Fogg, River-Aquifer Inter-  
861 actions, Geologic Heterogeneity, and Low-Flow Management, *Ground*  
862 *Water* 44 (2006) 837–852.
- 863 [62] D. J. Irvine, R. H. Cranswick, C. T. Simmons, M. A. Shanafield, L. K.  
864 Lautz, The effect of streambed heterogeneity on groundwater-surface  
865 water exchange fluxes inferred from temperature time series, *Water*  
866 *Resources Research* 51 (2015) 198–212.
- 867 [63] U. Schwartz, Factors affecting channel infiltration of floodwaters in  
868 Nahal Zin basin, Negev desert, Israel, *Hydrological Processes* 30 (2016)  
869 3704–3716.
- 870 [64] Y. Xie, P. G. Cook, P. Brunner, D. J. Irvine, C. T. Simmons, When  
871 Can Inverted Water Tables Occur Beneath Streams?, *Groundwater* 52  
872 (2014) 769–774.
- 873 [65] G. Gianni, J. Richon, P. Perrochet, A. Vogel, P. Brunner, Rapid identifi-  
874 cation of transience in streambed conductance by inversion of floodwave  
875 responses, *Water Resources Research* 52 (2016) 2647–2658.
- 876 [66] J. Batlle-Aguilar, P. G. Cook, Transient infiltration from ephemeral  
877 streams : A field experiment at the reach scale, *Water Resources Re-*  
878 *search* 48 (2012) W11518.
- 879 [67] A. S. Arrigoni, G. C. Poole, L. A. K. Mertes, S. J. O’Daniel, W. W.  
880 Woessner, S. A. Thomas, Buffered, lagged, or cooled? Disentangling  
881 hyporheic influences on temperature cycles in stream channels, *Water*  
882 *Resources Research* 44 (2008).
- 883 [68] F. P. Gariglio, D. Tonina, C. H. Luce, Spatiotemporal variability of hy-  
884 porheic exchange through a pool-riffle-pool sequence, *Water Resources*  
885 *Research* 49 (2013) 7185–7204.
- 886 [69] H. Roshan, G. C. Rau, M. S. Andersen, I. R. Acworth, Use of heat  
887 as tracer to quantify vertical streambed flow in a two-dimensional flow  
888 field, *Water Resources Research* 48 (2012).
- 889 [70] F. Gallart, N. Prat, E. M. Garca-Roger, J. Latron, M. Rieradevall,  
890 P. Llorens, G. G. Barbera, D. Brito, A. M. De Girolamo, A. Lo Porto,  
891 A. Buffagni, S. Erba, R. Neves, N. P. Nikolaidis, J. L. Perrin, E. P.

892 Querner, J. M. Quinonero, M. G. Tournoud, O. Tzoraki, N. Skoulikidis,  
893 R. Gamez, R. Gomez, J. Froebrich, A novel approach to analysing the  
894 regimes of temporary streams in relation to their controls on the com-  
895 position and structure of aquatic biota, *Hydrology and Earth System*  
896 *Sciences* 16 (2012) 3165–3182.

897 [71] J. D. Hunter, *Matplotlib : A 2D Graphics Environment*, *Computing in*  
898 *Science & Engineering* 9 (2007) 90–95.